Republic of Iraq
Ministry of Higher Education and
Science Research
University of Babylon
College of Engineering
Environmental Engineering
Department

MODELING OF AIR-WATER HEAT EXCHANGE IN SURFACE WATER BODIES: ALGORITHMS AND APPLICATIONS

A thesis
Submitted to the College of Engineering at the University of Babylon as a Partial Fulfillment of the Requirements for the Degree of Master of Science in Engineering/ Environmental Engineering

By

Dahlia Saad Abed-Zaid Jadoo

Supervised by

Asst. Prof. Dr. Hussein A. M. Al-Zubaidi

بسم اللَّهِ الرَّحْمَنِ الرَّحِيمِ

﴿ وَاللَّهُ خَلَقَ كُلَّ دَابَّةٍ مِنْ مَاءٍ ۖ فَمِنْهُمْ مَنْ يَمْشِي عَلَىٰ بَطْنِهِ وَمِنْهُمْ مَنْ يَمْشِي عَلَىٰ رِجْلَيْنِ وَمِنْهُمْ مَنْ يَمْشِي عَلَىٰ أَرْبَعٍ ۚ يَخْلُقُ اللَّهُ مَا يَشَاءُ ۚ إِنَّ اللَّهَ عَلَىٰ كُلِّ شَيْءٍ قَدِيرٌ ﴾

صدق الله العلي العظيم

سورة النور، الآية (45).

Supervisors' Certification

I certify that the preparation of this thesis "**Modeling of air-water heat exchange in surface waterbodies: Algorithms and applications**" was prepared "Dahlia Saad Abed-Zaid" under my supervision at Environmental Engineering Department/ College of the Engineering/ University of Babylon, as partial fulfillment of the requirements for the degree of Master in Engineering/ Environmental Engineering.

Signature:

Name**: Asst. Prof. Dr. Hussein A. M. Al-Zubaidi (Supervisor)**

Date: / 1 / 2022

Examining Committee's Certification

We certify that we have read this thesis entitled " **Modeling of air-water heat exchange in surface waterbodies: Algorithms and applications** ", and as an examining committee, examined the student "Dahlia Saad Abed-Zaid" in its content and in what is connected with it and that our opinion, it meets the standard of a thesis for the Degree of Master of Science in Environmental Engineering.

Signature:
Name: ***Prof. Dr. Nisren Jasim Al-Mansori*** *(Chairman)*
Date: / 1 / 2022

Signature:
Name : ***Prof. Rasha Salah Al-Kizwini*** *(Member)*
Date: / 1 / 2022

Signature:
Name: ***Asst. Prof. Dr. Ahmed Samir Naji*** *(Member)*
Date: / 1 / 2022

Signature:
Name: ***Asst. Prof. Dr. Hussein A. M. Al-Zubaidi*** *(Supervisor)*
Date: / 1 / 2022

Signature:
Name: ***Asst. Prof. Dr. Hussein Ali Mahdi Al-Zubaidi***
Address: Head of the Environmental Engineering Department
Date: / 1 / 2022

Approved by the Deanery of the College of Engineering.

Signature:
Name: ***Prof. Dr. Hatem Hadi Obeid Al-Taei***
Address: Dean of College of Engineering
Date: / 1 /2022

SUMMARY

Accurate estimation of surface heat exchange and its components is the basis for simulating surface water quality, especially in lakes and reservoirs, because the direct heat transfer between water and air affects thermal stratification. In this work and based on high time resolution data of water surface temperature and meteorological parameters from Lawrence Lake (OR, US), the term-by-term method was used to model surface heat fluxes (solar and atmospheric radiation, back radiation, evaporation, and conduction) by using the MATLAB environment to develop the code and simulate the results. The developed model is considered as a stand-alone model and can be used by other authors to simulate temperature in surface waterbodies. The ability to highlight the contribution of each flux is the main feature of the model, providing evidence of the strong interaction between the water surface and the atmosphere. This interaction cannot be neglected in surface water quality modelling.

During the study period (487-670) Julian day, the results showed that summer solar energy was the highest intensity with a peak record of 842.05 Watt/m^2 at 540.91 Julian day. And because of the natural event of sunrise and sunset, solar energy has its daily fluctuation. It fluctuates between 0 Watt/m^2 at night and reaches its daily peak at approximately noon. Although the maximum value of evaporation heat flux was recorded at 578.44 Julian day (359.77 Watt/m^2), the minimum conduction value at 655.54 Julian day was (126.039 Watt/m^2). Back radiation fluctuates less than other fluxes. This returns to its dependence on one variable factor, which is water temperature. The maximum value, recorded to the back radiation, was (410.06 Watt/m^2) related to the maximum water temperature (21.5 ^oC). The simulation of the model highlighted

the influence of the solar radiation bell-shaped curve on the total heat flux curve.

In addition, the model implementation of Edinger's suggestion for wind speed coefficients (b1 = 9.4, b2= 0 and b3 =0.46) was used as a feature in the model to calibrate the total heat flux. It was found that the resulted curves of this calibration simulated the fluxes but in different ranges. For more flexibility, other suggestions from several wind functions were applied in the model. It was found that (Ahsan & Blumberg, 1999; Arifin et al., 2016; Ji, 2017) models were the closest to the Edinger's model. Furthermore, a wind sheltering coefficient (WSC) was proposed and taken into account as a multiplication factor of wind speed.

In order to link the developed model with the advection-dispersion equation, a case study was performed based on field data from an aeration basin located in Al-Muamirah wastewater treatment plant. Based on available data from the Al-Muamirah wastewater treatment plant, the model was run for 24 hours to estimate the temperature along the aeration tank. Some data has been enforced due to a lack of data related to the research location. After multiple trials, the hypothesis was validated. The predicted temperatures were very close to the real data. The MAE and RMSE were relatively low. It's also worth noting that the arrival of waste water heralds the start of a new heat wave, which steadily intensifies until it reaches the basin outlet, when it reaches its peak. With each entry, the process is repeated. The low errors values demonstrate the model was able to simulate the aeration basin temperatures efficiently. At 10 a.m. on 28/6/2021, the measured wastewater temperature at the middle of the tank was 30 ^{o}C and the estimated wastewater temperature at the middle of the tank was 29.81 ^{o}C. Moreover, several plots presented the estimated temperatures for the aeration basin for 24 hr were displayed.

DEDICATION

This dedicates this work for:

For God's sake

My great Prophet, Muhammad,

who has taught us the purpose of life.

To my dear husband,

Hussein Hamid.

To my beloved girls: Zainab and Zahraa.

Dahlia Saad

2021

ACKNOWLEDGEMENTS

"In the name of Allah the most Merciful and Compassionate"

Praise be to God for every blessing, whether it was still or not. And may God's peace and blessings be upon His Messenger, Muhammad the prophet.

I am grateful to everyone who helped me during this work especially my supervisor, Prof. Dr. Hussein Ali Mahdi Al-Zubaidi, for his guidance, and sharing his wealth of knowledge. Also, thanks to the Water Quality Group at Portland State University's Maseeh College of Engineering and Computer Science for their assistance with this research.

My warm thanks go to my little girls, my daughters. Also, I am indebted to my husband, Hussein Hamid. Your name should be on this work as much as mine. You were always there, wherever and whenever that was.

For their support and hope, they had given to me. My family, without that hope, this study would not have been possible. Many thanks and gratitude to everyone who gave help to carry out this study.

Dahlia Saad

2021

Table of Contents

List of Figures

List of Tables

List of Abbreviations

Abbreviation	Description
AME	Absolute mean error.
a	Empirical coefficients of wind speed function, $a = 9.4$ Watt /m^2/ mmHg.
b	Empirical coefficients of wind speed function, $b = 0.46$ Watt /m^2/ mmHg/(m/sec)^2.
c	Empirical coefficients of wind speed function, $c = 2$.
C_c	Bowen's coefficient (0.47 mmHg/ °C).
C_p	Specific heat of water at constant pressure.
D	Dispersion coefficient.
e_a	Atmospheric vapor pressure at $2m$ above the water surface (mmHg).
e_s	Saturated vapor pressure at T_s (mmHg).
$f(W)$	Wind speed function (Watt/m^2/ mmHg).
h	Waterbody depth.
H_a	Atmospheric long wave radiation (Watt/m^2).
H_{an}	Net atmospheric radiation (Watt/m^2), $H_a - H_{ar}$.
H_{ar}	Reflected Atmospheric long wave radiation (Watt/m^2).

H_{br}	Back long wave radiation (Watt/m^2).
H_c	Conduction heat flux (Watt/m^2).
H_e	Evaporation heat flux (Watt/m^2).
Jday	Julian day. The counting of days begins on the first day of the project.
NSE	Nash–Sutcliffe efficiency.
RMSE	Root mean square error.
R_h	Relative humidity.
T	Temperature.
t	Time.
T_a	Air temperature, °C.
T_s	Water temperature, °C.
T_d	Dew point temperature (°C).
u	Flow velocity.
W	Wind speed measured at $2m$ above the water surface (m/sec).
WSC	Wind sheltering coefficient.
W_z	Elevation of desired wind velocity (m).

W_{z1}	The known wind velocity (m/sec) at elevation z_1. (m).
X	Distance along the axis.
z	Elevation of known wind velocity (m).
z_0	Wind roughness height (m).
z_1	Elevation of desired wind velocity (m).
$(1 + 0.17C^2)$	Accounts for the cloud cover effect (Wunderlich, 1972).
ρ	Water density.
ϵ	Emissivity of the waterbody (0.97).
σ	Stefan-Boltzmann constant (5.62E-8 Watt/m^2/°k^4).
$\alpha_\circ$	A proportionality constant (0.937E-5).

CHAPTER ONE

Introduction

1.1 Introduction

The prerequisite for an accurate understanding of aquatic ecosystems is knowledge of thermal systems. For aquatic beings, the most important parameter is the existence of dissolved oxygen (Taft, 1958). The dissolved oxygen rate (DO) reduces as the water temperature increases. DO and water temperature have an adverse relationship. This relation has been subjected to various studies (Steele, 1989;Kalinowska & Rowiński, 2015; Kuligiewicz et al., 2015). Demars et al., (2011) worked on temperature effects on the respiration of the entire stream ecosystem and showed that "The temperature is an essential (but not alone) driver of stream and rivers metabolism". Regardless of the technicalities, any change in water temperature will have severe implications. Re-oxygenation and decomposition rates of organic waste will be affected by increasing water temperature, which will alter dissolved oxygen profile (Demars & Manson, 2013).

Oxygen is very necessary to metabolism; therefore, if the temperature of water rises, some species may disappear completely. This fact alone has become the purpose of many studies related to the heat balance of water bodies. Heat budget has critical importance and cannot be neglected when the aquatic ecosystem health is under investigation. One of the most essential elements in ecosystem research is water temperature. Temperature affects biological and chemical activity such as dissolved oxygen concentrations, fish development, and even mortality. Another fact is that in the alligators' case and several reptiles, the temperature is the crucial factor for determining gender during egg incubation (Murray, 2002). Any change in water temperature will affect those species' sex ratio, which is important for population dynamics and survival (Kalinowska & Rowiński, 2015).

Water has a unique property which is absorbing thermic energy while witnessing only slight temperature changes. Unfortunately, most aquatic species

have strengthened enzyme systems that function in narrower temperature ranges as a result of this characteristic. Relatively a minor change in natural environmental temperature can lead to considerable environmental problems. For instance, a rise in water temperature can knock off fishes that are heat intolerant in severe situations. This comprises plants hinder the aquatic food chain's web of life (Kalinowska & Rowiński, 2015).

Furthermore, many biological conditions are influenced by the river water temperature. The temperature of the water, for example, has a significant impact on the spawning period of sockeye salmon. Authors found when the temperature touched 19 ^{o}C, spawning had been disturbed by the thermal cover of individual fish (Reiser & Bjornn, 1979). Salmon fish mortality rate increases due to the increases in stream temperatures (23-25°C). Johnson (1997) linked water temperatures to the Atlantic salmon fry emergence timing (Benyahya et al., 2007).Some researchers discussed the human impact of river thermal conditions. For instance, Beschta et al., (1987) worked on the river water temperature in forestry conditions. Also, Webb & Walling (1993) studied the reservoir's downstream effects. Changes in bank land cover, which influences shade on the water surface, river morphology, which affects the surface area, water depth, and velocity rate, and the link between flow and groundwater, storm water, and other inputs can all help to raise water temperatures. When precipitation strikes hot impermeable surfaces of civil areas, the result is warmer storm water than the water temperature.

Finally, the heat exchange affects the heating system and valuable elements include climatic and physical properties. The meteorological factors such as air temperature, wind speed, humidity, etc. affect the air-water energy exchange. In addition, this exchange is influenced by the annual cyclic of incoming short radiation, riparian vegetation (especially in tiny water streams), stream perspective, canal geomorphology, the topography of the valley,

tributary positioning, and groundwater inputs. Changes in water temperature are essential to aquatic resources, both temporally and geographically (Vannote et al., 1980). Human interventions such as deforestation and dam control frequently disturb these processes (Webb & Walling, 1993). For further illustration, bank vegetation that is affected by forest processes will have a large impact on the river heat flux budget components (Brown & Krygier, 1970; Hilaire et al., 2000). The temporal and geographical variability of water temperatures is influenced by flow variations and/or water withdrawal (Sinokrot & Gulliver, 2000). In a recent study, the interconnection of air and water temperatures were more intense when the discharged flow was beneath the annual average (Gu et al., 1998; Webb et al., 2003).

1.2 Statement of problem

Thermal pollution in the aquatic system is the result of processes that vary the surrounding temperature in water bodies. Any change in ambient temperature in nature even if it is very small can cause serious environmental problems. This change in the temperature of water may pass the natural fluctuation limit of temperature. Therefore, it is necessary to make predictions of water temperature fluctuations and environmental impact assessments including air-water heat exchange in details.

1.3 Engineering Significance

The study is significant in addressing the role of air-water surface heat exchange in the modeling of thermal pollution. This study is one of the essential steps for implementing the advection-diffusion equation accurately. This work has a role in the sinks/sources calculation in the mentioned equation. It helps researchers who are focusing on the assessment of the water temperature and its

influence on the aquatic system, and may also be used for heat distribution investigation in surface water bodies. In addition, it assist in predicting and evaluating future developments in water temperature variations before every industrial building that disposes heat into waterbodies.

1.4 Objectives of the study

The main objectives are:

1. To build a model capable of calculating air-water surface heat exchange fluxes.
2. To perform a sensitivity analysis for several parameters in the model.
3. To regress air and water temperatures of surface water bodies.
4. To implement the developed model by doing a real case study.

CHAPTER TWO

Theoretical Concepts
and
Literature Reviews

2.1 Introduction

Most of the earth is covered by water. From this point of view, the importance of water studies comes. There are many studies in different majors about water. The study of water quality and climate change is one of the most popular topics about water. There is some sensitiveness of water quality perspectives to climate change, and water temperature is the most critical water feature. Any increase in water temperature leads to a decrease in dissolved oxygen transfer rate to the water column. In turn, the latter will impact the biological activity of the water body ecosystem.

As the sun rises every morning, its rays heat everything including surface water and air. Water layer that is next to the air layer will get a portion of that heat, and some of this heat will be lost by evaporation and conduction. A portion of solar radiation is reflected from water to the atmospheric layer. Also, the water surface emitted radiation and in turn it contributes to the cooling of water. Figure (2-1) shows that graphically. Table (2-1) summarizes fluxes typical values. The mentioned five fluxes together contribute to make the net total surface heat flux (H_t). In turn it becomes the heat transport equation sink/source, see eq. (2-1).

$$\frac{\partial T}{\partial t} + u\frac{\partial T}{\partial X} = D\frac{\partial^2 T}{\partial X^2} + \frac{H_t}{\rho . C_p . h} \quad \dots\dots\dots\dots\dots (2-1)$$

Where

T: Temperature.

t: Time.

u: Flow velocity.

X: Distance along the axis.

D: Dispersion coefficient.

H_t: Net heat exchange flux.

ρ: Water density.

C_p: Water specific heat at a constant pressure.

h: Water body depth.

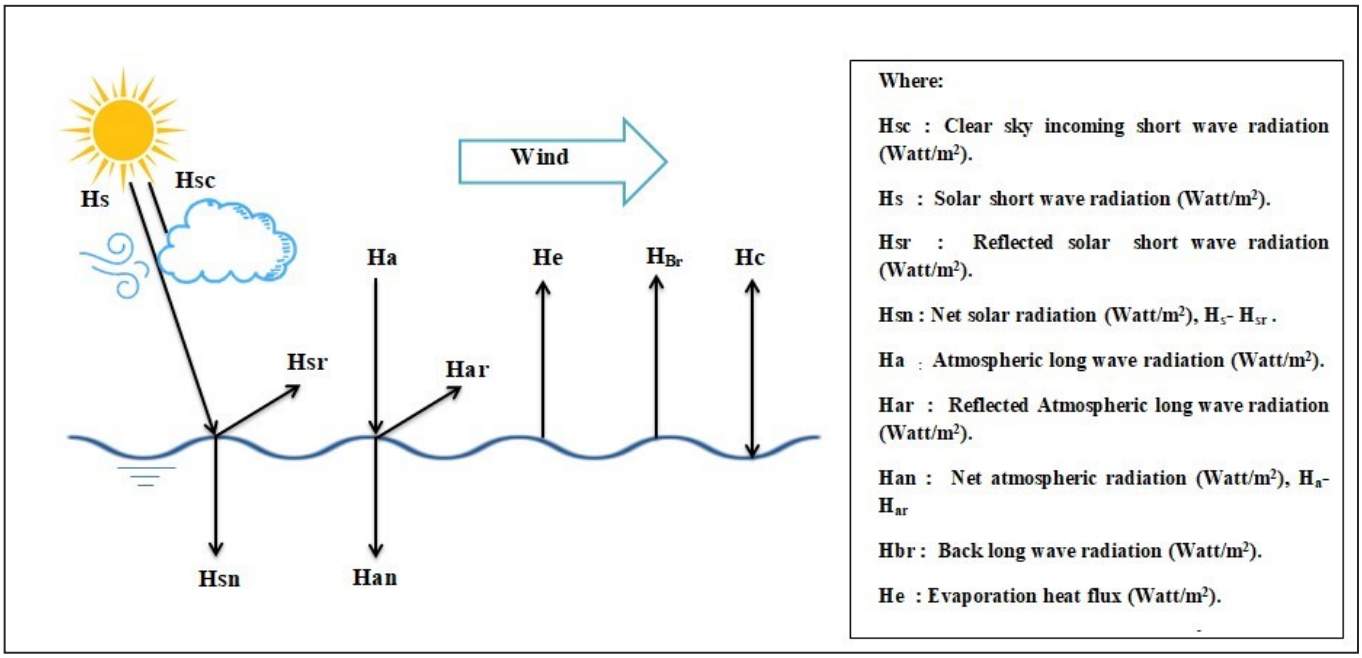

Figure (2-1): Surface heat exchange components

Table (2-1): Typical values for the surface heat exchange components according to (Al-zubaidi 2018; Kalinowska 2019):

Fluxes	***Fluxes typical values (Watt/m^2)***
Solar radiation	(50 – 350)
	For a sunny day, (800 – 1000)
	For a very cloudy day,(100 – 300)
Atmospheric radiation	(200 – 400)
	(30 – 450)
Back radiation	(250 – 500)
	(300 – 500)
Evaporation	(0 – 35)
Conduction	(–70 – 200)

2.2 Previous related literature

Al-Zubaidi & Wells (2020) developed a 3D hydrodynamic and water quality model to predict the temperature and water quality constituents transport in surface waterbodies. Comparisons between the model predictions and the analytical solutions and field data were performed to validate the model. The surface heat fluxes were calculated based on Cole and Wells (2017) and Edinger et al. (1974). The net solar shortwave radiation determination was based on Wunderlich (1972). The 3D model can either compute clear-sky solar radiation theoretically and adjust it by cloud cover or read in measured short-wave solar radiation directly from the available meteorological data. The net atmospheric long-wave radiation was computed by an approach proposed by Wells et al. (1982). For air temperature greater or equal to 5°C, the atmospheric clear-sky long-wave radiation was calculated using the approach of Swinbank (1963). For air temperature less than 5°C, the atmospheric clear-sky longwave radiation was calculated by adopting the approach of Idso and Jackson (1969). Back (Long Wave) Radiation, evaporation heat flux, and conducted heat fluxes from the water surface were computed using the approach proposed by Cole and Wells (2017). Finally, the results of total net heat fluxes were used to calculate the temperature and water quality sources/sinks. As a result, the 3D model showed good agreement with field data.

Abdi & Endreny (2019) developed the i-Tree Cool River mechanical model and tested whether it can determine the cause of thermal pollution and mitigation measures. The model represents the influence of external loads that receive solar radiation without river bank shelter, multiple lateral rainwater channel flows, tributaries of drainage reservoirs, groundwater flow, and low levels of constant flow in dry climates and unstable flow in humid climates. The i-Tree Cool River model simulates a convection-diffusion equation with inflow and heat transport. The long-wave radiation flux composes of two fluxes. The

first is a positive downward flux from the atmosphere and land cover over the water surface. The other is a negative rising flux from the water body. Atmospheric long-wave radiation was calculated by applying (Boyd & Kasper, 2003). The emissivity of the atmosphere was calculated by the use of the Kustas equation. The general sky-view-factor formula was computed based on (Chen et al., 1998). Land cover radiation trace the approach of the land cover of (Boyd & Kasper, 2003). Water body is influenced by air radiation, depending on the water temperature in which the heat flow adopting the approach of (Boyd & Kasper, 2003)..

Kalinowska (2019) studied the workable difficulties associated with the thermal spread in the river. The author attempted to outline and discuss probable challenges with the understanding and practice of water-air exchange calculations. Water temperature measurements was for the Narew and Świder rivers, in Poland, which is have different characteristics. Edinger's equation was used to calculate the total heat budget. The shortwave solar radiation was calculated based on the Magnusson et al. (2012) equation and then corrected, taking into account the shading. The incoming shortwave solar radiation was measured from three different meteorological stations for the both rivers, resulting in different values. This difference could be due to the effect of the riverbank vegetation. The incoming atmospheric radiation was estimated according to the modified Stefan-Boltzmann equation, and the main difficulty was the calculation of the emissivity of the atmosphere. The author used several formulas to calculate the atmospheric emissivity for different sky conditions. Evaporation and condensation were calculated based on the Dalton equation, where the saturated vapor pressure at the surface of the water was calculated using the Magnus formula (Magnus, 1844). For wind speed function, the author calibrated the chosen wind speed formula by applying and comparing several equations using meteorological data from local measurements. Conduction and

convection processes were obtained by adopting Bowen ratio (Bowen, 1926; D. N. Moriasi et al., 2007; Bowen, 1926; Ji, 2017). In addition, this technique lowers the quantity of input data needed.

Kalinowska & Rowiński (2015) worked on a stream temperature modeling framework, especially after a significant quantity of heat pollution was introduced. The exchange mechanisms between the river water and its environment also was examined, and the circumstances arising from unanticipated fluvial shift in thermal conditions were taken into account. The heat exchange equation was written based on (Edinger et al. 1974; Rutherford et al. 1993). All components were calculated based on hydrological data, the temperate of water, and meteorological data. The heat exchange equation became a complicated nonlinear water temperature function, and then the solution of the heat transport equation were converted to a linear form.

Fink et al. (2014) looked for significant changes in heat exchange process with the environment, as well as their temporal evolutions. For this reason, a model was used to a large Central European lake linked by the Rhine River and consists of two basins. Two sets of data were collected per month at the lake deep bottom point, and surface water temperatures were measured continuously at other places. This information was utilized to create surface water temperature continuous time series measurements. The difference between the two temperatures was calculated for all. The temperatures of the river water were measured at a measuring Constance station. The station provided the required daily average measurement data for the years 1981–2011. The entire sum of all heat fluxes is the net heat flux. Downward fluxes are considered positive, and vice versa. A dispersed light cloud and a moderately disturbed water surface were used to calculate shortwave absorption based on Cogley (1979). The absorption of the atmospheric radiation is represented by Stefan-Boltzmann law. The emissivity is specified by humidity and clouds with

a calibration parameter. Stefan-Boltzmann law was adopted to obtain lake surface atmospheric radiation at the absolute temperature of the water. The surface emissivity (0.972) was utilized in this study. Dalton's law, which is widely used, was adopted for evaporation and conduction. The saturated water vapor pressure was approaching by the Magnus formula. The wind velocity was calculated by using Kuhn (1978). Forced and free convection (Bowen, 1926) was based on Livingstone and Imboden (1989) by inserting equation (Dalton's law) into the equation (Bowen, 1926).

Prats et al. (2012) used the technique of equilibrium temperature, and the hydrological years for various seasons and hydrologic years were used. Furthermore, the thermic change of heat fluxes is addressed. A temperature monitoring program was conducted downstream of the Ebro River. A lot of researches, including this one, has been conducted on this area to look for the impact of the thermal change resulting from the nuclear plant on the river ecosystem. A modeling technique was validated by comparing the measured temperature with the simulated water temperature. Net short wave radiation was determined based on the method suggested by Campbell and Aarup (1989). Net longwave heat flux was estimated based on one of the parameterizations achieved by Aubinet (1994), while long-wave radiation released by the water surface was determined by adopting the usual grey body formula with emissivity of 0.97. Evaporative heat flux was gained using Sill (1983) method. At last, convection was calculated based on the Bowen ratio (Henderson-Sellers, 1986). The numerical model was built in the MATLAB environment to evaluate longitudinal hydrodynamic and heat fluxes within selected sections of the Ebro River.

Christopher et al. (2010) predicted the longitudinal temperatures changes using the heat budget model. This research also describes the transverse and daily variations in Waikato River temperature, the longest river in New

Zealand. Meteorological data were taken hourly from two locations. Global measurements of radiation were also provided every hour. Model equations were solved using the STATS program. Evaporation was estimated using three models. Then the model was developed using Jobson (1977) and meteorological data from the second location. Temperatures downstream were estimated and compared to typical naturalistic transverse temperatures. The net heat flux was calculated by Edinger et al. (1974). Short wave flux was assumed eighty percent direct, and the rest was diffused. Surface reflectivity was produced by coefficients that change with cloud cover and solar height. Evaporation was calculated based on water density, vapor latent heat, the air-saturated vapor pressure at the surface water temperature, and air vapor pressure. Different experimental formulas have been acquired from field data to predict wind speed function. TVA (1972) was applied to estimate the function of wind speed. Also, Jobson (1975) and (Jobson 1977) were utilized to calculate the function of wind speed. The evaporation estimation of all formulas has given the same results. Vapor pressure of the air was retrieved from humidity and dry bulb air temperature. Alternatively, the vapor pressure of the air was determined from wet and dry-bulb air temperature. Conduction heat flux was obtained using the Bowen ratio, and back-radiation was determined by Stefan-Boltzmann ratio with emissivity of 0.97.

Foreman et al. (1995) built a model for predicting temperature in the Fraser River as well as the major Sockeye tributaries. This was an investigation study to examine the ability of cold water coming from the lake to lower the temperatures of the waters of the Fraser River. The Fraser River is Canadian largest river and drains into the Pacific Ocean. The river source is near Jasper, Alberta in the Rocky Mountains. it has 1370 km journey to the Strait of Georgia. The researchers used (Edinger et al., 1974) to calculate the net rate of heat flux. Magnusson equation with albedo of 0.06 was used to calculate

shortwave radiation, and Siwmbank was used for computing longwave radiation. Back-radiation was obtained using Stefan's Law with water emissivity of 0.96. Dalton's equation was used for the evaporation rate computations. Magnus empirical formula was used for both air vapor pressure and saturated air vapor pressure. Also, wind function was calculated based on Shanadan 1985 equation with the evaporation constants (a= 9.2, b=0.46, c=2). Finally, for conduction heat loss, Bewon's equation was adopted.

Shanahan (1984) reviewed the techniques for the computation of water temperature in surface water bodies. The review described various styles for dealing with input data and units to forecast net heat transfer based on two approaches: the complete thermal budget and the linear heat exchange. Edinger's equation was applied to calculate the net flux. The author suggested Wunderlich (1972) method with a factor of 0.94 to account for the average reflectance of the water surface and calculate solar radiations. Brunt's formula (Brunt, 1932) and Stefan-Boltzmann ratio of a factor of (4×10^{-8}) were used as multiplying water emissivity and Stefan-Boltzmann constant for atmospheric radiation and Back Radiation. For wind function, several equations were used as shown in Table (2-2).

Table (2-2): Wind functions conditions (Shanahan, 1984).

Equation	***Condition***
Lake Hefner equation Harbeck (1952)	Natural Lakes
Meyer (1942)	Natural Ponds and Lakes
USGS/Chattahoochee River Barnwell (1982)	Natural River
QUAL-II Roesner et al. (1977)	Rivers
Brady, Graves and Geyer (1969), Ryan and Harleman (1973) & Throne (1951).	Cooling Ponds
Rimsha and Donchenko (1957)	Heated Streams in Winter

2.3 Literature gap and model features

Based on the advantages and disadvantages of the models listed in the literature above, a MATLAB model was built to calculate heat exchange fluxes between air and water surface. The model could be applied to any surface waterbody after entering the required metrological data. Taking the advantages of Edinger et al. (1974) and Cole and Wells (2017), surface heat fluxes were calculated to be used in the calculation of the source/sink term of the heat transport equation. The EPA model was used to calculate solar radiation. This EPA model was included in the CE-QUAL-W2 water quality model and showed high agreement with field data. Atmospheric net radiation was obtained using Wells et al. (1982). The adopted equation for the back radiation calculation was (Steven C. Chapra, 2008) with water emissivity value of 0.97 (the most reliable value). Wind speed profile was calculated based on Edinger et al. (1974) suggestion

after correcting wind speed. The correction was done based on Ryan and Harleman (1973). Then evaporation heat flux was obtained (Cole & Wells, 2006). Conduction calculation was obtained by the Bowen ratio (Cole & Wells, 2006; Kalinowska, 2019). Several features were required to be presented together to add more strength and flexibility in the computations. These features are:

1. Wind sheltering coefficient needs to be added to overcome the deference between metrological station wind speed reads from different locations.
2. Flexibility is required to calculate the wind speed profile from different functions.
3. The ability to make a calibration for Edinger equation's coefficients in any rage with intervals is required.
4. Retrieve water temperature from air temperature from different models such as logistic and sinusoidal regression models will be a useful tool.
5. In addition, MATLAB can determine the following directly:
    A. AME and RMSE errors.
    B. Maximum, minimum and mean fluxes values.

Laurance lake was selected to build the model because it has a high resolution metrological data. Laurance Lake is a reservoir situated at the Mountain Food base in the County of Hood River, Oregon, USA (Berger et al., 2005; Al-Zubaidi, 2018). Linear interpolation was performed due to the difference in time intervals between water temperature data and metrological data. In addition, the model was applied to the aeration tank of the wastewater treatment plant in Al-Muamirah. The plant is located in Muamirah, south of the city of Hilla, the province of Babylon, Iraq. The model was linked advection-dispersion equation adopted for the model (Makinia et al., 2005). Three additional fluxes were added. The three fluxes are (aeration, biological and mechanical heat fluxes). Aeration heat flux was obtained as (Talati &

Stenstrom, 1990). Biological heat flux can be figured based on Gibb's free energy terms (Wells et al., 2005). Mechanical heat flux was computed as (Makinia et al., 2005). The model ran for 24 hours to estimate the temperatures in the aeration tank based on the available data from Al-Muamirah wastewater treatment plant. Due to a lack of data in the study location, some data has been assumed in its typical range. The estimated wastewater temperatures have a difference less than 0.5 ^{O}C.

CHAPTER THREE

Methodology

3.1 Introduction

The prerequisite for an accurate understanding of aquatic ecosystems is knowledge of thermal systems. For aquatic beings, the most important parameter is the existence of dissolved oxygen (Taft, 1958). The dissolved oxygen rate (DO) reduces as the water temperature increases. DO and water temperature have an adverse relationship. This relation was subjected to various studies (Steele, 1989). Recent studies have revealed that the water temperature and dissolved oxygen rate relationship under specific conditions is a hysteretic style (Monika B. Kalinowska & Rowiński, 2015; Rajwa-Kuligiewicz et al., 2015). Demars et al. (2011) worked on temperature effects on the respiration of the entire stream ecosystem and showed that "(The temperature is an essential (but not alone) driver of stream and rivers metabolism)". Regardless of the technicalities, any change in water temperature will have severe implications. Re-oxygenation and decomposition rates of organic waste will be affected by increasing water temperature, which will alter dissolved oxygen (Demars & Manson, 2013).

3.2 Location and background of the research area

Laurance Lake is a reservoir situated at the Mountain Food base in the County of Hood River, Oregon, USA (Fig. (3-1)). Its latitude and longitude coordination are 45.46 and 121.66, respectively. It has an elevation of 910m above sea level. It was built for irrigation conservation in 1968. At its full Pool, it has a capacity of 3564 acre-feet (Berger et al., 2005; Al-Zubaidi, 2018). Reservoir inflows flow into the major inflows from Clear Branch Creek at the western end of the reservoir and into smaller inflows at Pinnacle Creek in the southeastern corner of the reservoir. There is a dam and outlet at the eastern end of the reservoir (Al-Zubaidi, 2018).

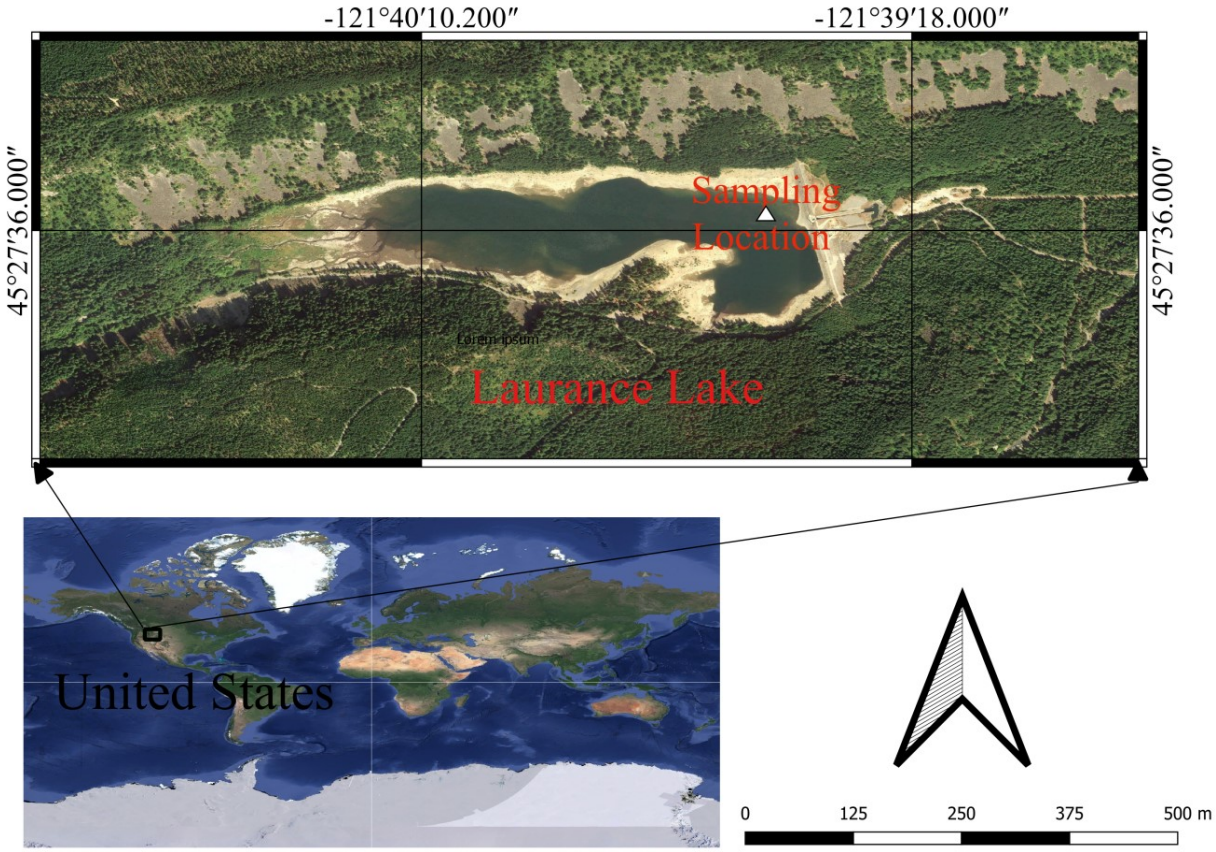

Figure (3-1): Laurance Lake, Oregon, USA location (retrieved from Google by QGIS).

3.3 Model input data and Code algorithms

Meteorological data are required to activate the code. Air and water temperatures, dew point, wind speed, relative humidity, and cloud cover were all the inputs. The model can handle input data from various time intervals. Two datasets were used to run the model. One dataset is linked to the input meteorological data, while another is linked to the surface temperature of the waterbody. Each dataset has a various time resolution. The available surface water temperature was at the dam and had a different temporal resolution than the meteorological data. As a result, linear interpolation was employed to calculate surface water temperature at any required time. Based on water temperature, back radiation was calculated. While atmospheric radiation calculation depends on air temperature and cloud cover. Evaporation estimation

is done based on water temperature, dew point, relative humidity, and wind speed profile. Wind speed is corrected, and then it enters the calculation of the wind speed profile. For code activation purposes, Laurance Lake meteorological data are adopted. The data was measured at two stations. The first is at the dam and the other is at a station at Parkdale. Datasets cover the period (487-670) Jday (Julian day) where the first Jday is at 1/1/2002 (Berger et al., 2005). The theoretical framework was presented in Fig (3-2). Figure (3-3) is a summarized schematic flowchart for the code.

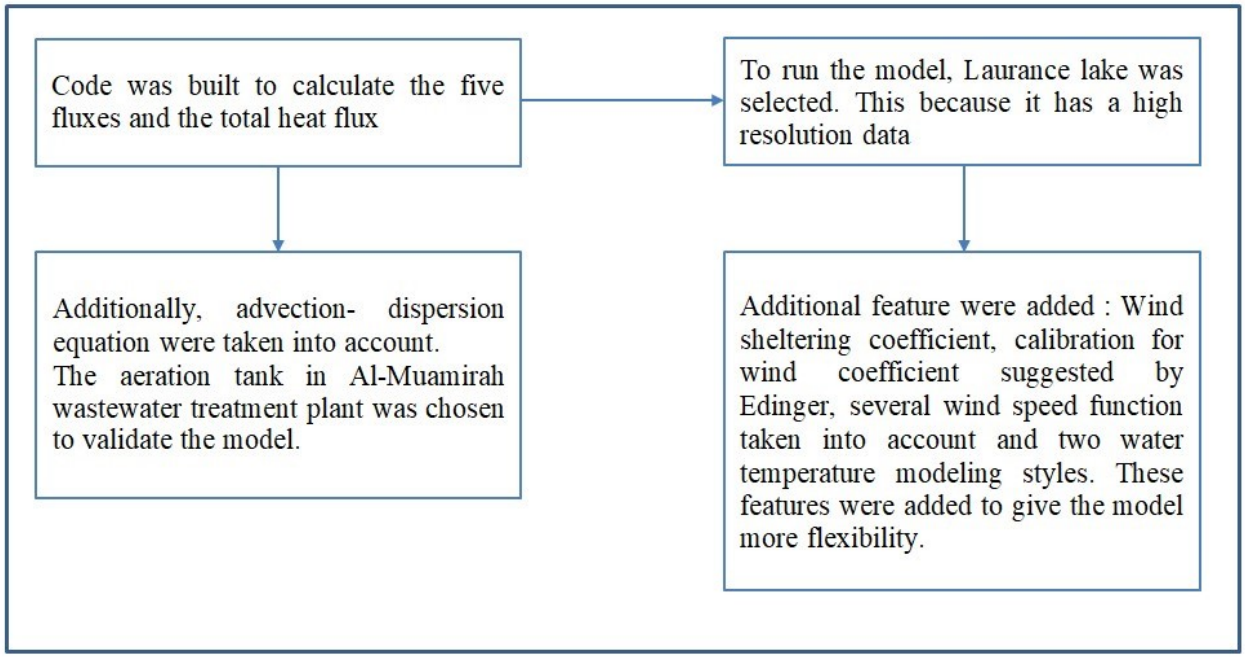

Figure (3-2): Theoretical framework.

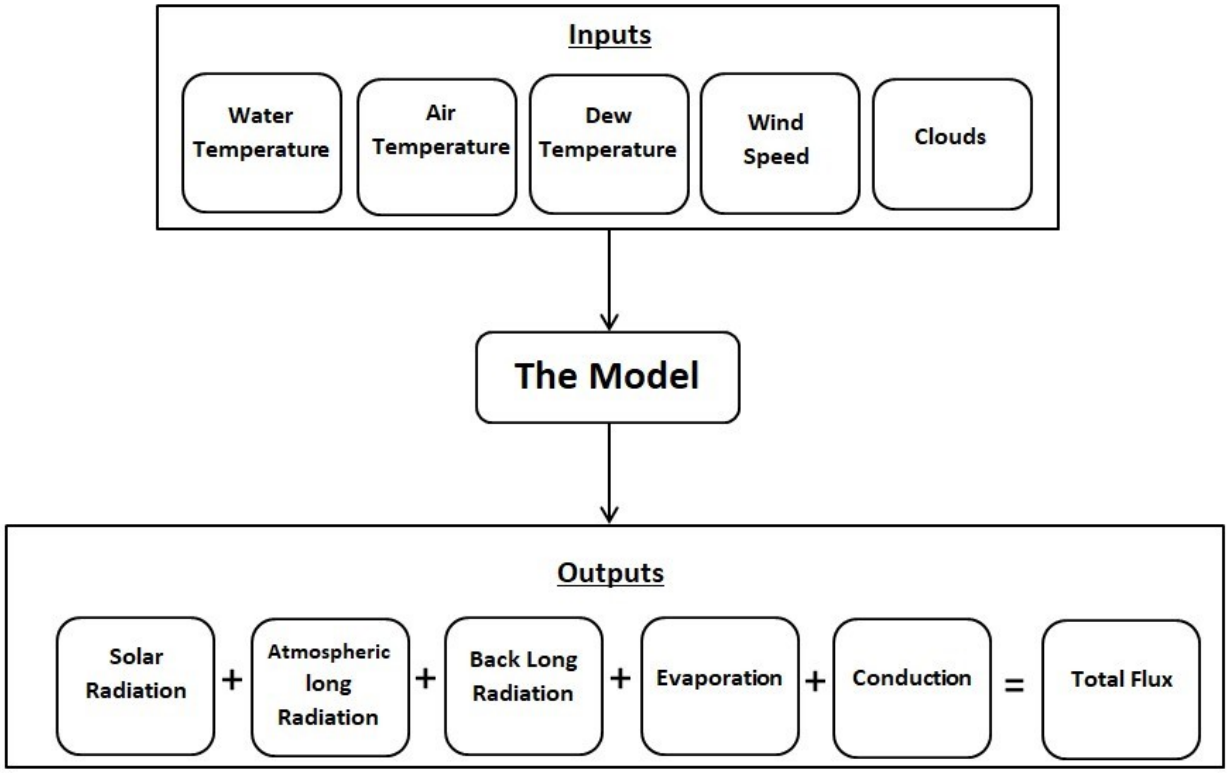

Figure (3-3): MATLAB code summarization.

3.4 Model fluxes calculations

Surface heat fluxes are estimated by applying the method in Cole and Wells (2017) suggested by Edinger et al. (1974). Consequently, the net surface heat flux (H_t) in Watt/m^2 and as follows (Foreman et al., 1997) :

$$H_t = H_{sn} + H_{an} - H_{br} - H_e - H_c \quad \ldots\ldots\ldots\ldots\ldots (3-1)$$

Where (H_t) can be used for the calculation of the source/sink term of the heat transport equation (eq. 2-1).

3.4.1 Solar Radiation

Short wave radiation comes from the sun (Grossnickle & Canada, 2000). It is the most valuable factor that rules both seasonal and daily water temperature variations (Al-Murib et al., 2017). On the surface of this planet, solar radiation is greatly unsteady spatially and temporally. However, it is nearly constant in

the upper atmosphere of the earth with a value of 1370 Watt/m^2 and is called the solar constant (Klassen & Bugbee, 2015).

Special filtering is being made of the spectrum quality and amount of radiation delivered to the earth through the atmosphere. Moisture, gases, and particle matter in the air scatter and absorb, resulting in filtration. The residual radiation is dispersed or absorbed by water, CO_2, ozone, and particulate matter. Solar radiation is divided into two types: direct and diffuse. Global radiation is the sum of the two. Direct normal irradiance (DNI) is the straight-line radiation from the sun (Klassen & Bugbee, 2015). The magnitude of short-wave radiation counts on several factors: solar altitude, scattering and absorption, reflection, and shading (Steven C. Chapra, 2008). Solar radiation ranges (800-1000) Watt/m^2 for sunny days. While for cold winter days, solar values have a domain of (100-300) Watt/m^2 (Kalinowska, 2019).

There are many models for calculating and estimating solar radiation such as the model proposed by Klein, 1948; Kennedy, 1949; EPA, 1971; and Lee, 1978; Meeus [1999] and (Annear & Wells, 2007). In this thesis, the EPA model was admitted. This model has been used in the water quality model CE-QUAL-W2 and presented a good agreement with field data. All the equations used for estimating the sun position have been refined based on updating the original formulation given in EPA (1971) and (Cole & Wells, 2006).

3.4.2 Atmospheric radiation

Atmospheric long-wave radiation is the radiation that results from the absorption and re-radiation of solar short-wave radiation, mainly by water drops and vapor in the atmosphere. It depends on cloud cover and cloud altitude (Foreman et al., 1997; Wang & Dickinson, 2013). Both short-wave solar and long-wave atmospheric radiations are not a fashion of water temperature and are submitted to be scattered and reflected at the interface of air and water

(Foreman et al., 1997). While the solar radiation measurements are comparatively available from numerous meteorological stations, the long-wave radiation measurements are computed. Atmospheric long-wave radiation value depends on the air temperature and differs between (30-450) Watt/m^2 (Kalinowska, 2019). Whereas Al-Zubaidi (2018) stated that the magnitude of long-wave radiation is in the range of (200-400) Watt/m^2 .

Atmospheric net radiation (H_{an}) can be obtained using Wells et al. (1982). With the addition of the cloudiness and the reflectivity effect, the final adopted equation for calculating the net long-wave radiation can be written as mentioned in (Al-Zubaidi, 2018):

For air temperature (Ta) ≥ 5 °C:

$$H_a = \epsilon\sigma\alpha_\circ(T_a + 273)^6(1 + 0.17C^2) \ \dots\dots\dots\dots\dots(3-2)$$

For air temperature (Ta) < 5 °C:

$$H_a = \ \epsilon\sigma\alpha_\circ\ (T_a + 273)^6\left[1 - 0.26e^{(-7.77E-4T_a^2)}\right](1 + 0.17C^2) \ \dots\dots\dots\dots(3-3)$$

Where

ϵ: is the emissivity of the waterbody (0.97)

σ: is the Stefan-Boltzmann constant (5.62E-8 Watt/m^2/°k^4).

$\alpha_\circ$: is a proportionality constant (0.937E-5).

T_a: is the air temperature (°C).

(1+ 0.17C^2): accounts for the cloud cover effect (Wunderlich, 1972).

3.4.3 Back-radiation

Likewise, earthly objects waterbodies emit long-wave radiation, which contributes to cool down from the water surface. The value of back radiation

heat flux usually fluctuates within (300-500) Watt/m^2 (Deas & Lowney, 2000). With the assumption that water temperature is available, the calculation of back radiation is relatively easy. Back radiation calculation is similar to the long-wave atmospheric radiation calculation fashion. It could be computed based on Stefan Boltzmann's law, but with different emissivity. The water emissivity value is between 0.9 to 0.99, but 0.97 is the most reliable value (Kalinowska, 2019). The adopted equation for the back radiation calculation is (Steven C. Chapra, 2008):

$$H_{br} = \epsilon\sigma\alpha_{\circ}(T_s + 273)^6 \quad \ldots\ldots\ldots\ldots\ldots (3-4)$$

Where
ϵ : is the emissivity of the waterbody (0.97).
σ: is the Stefan-Boltzmann constant (5.62E-8 Watt/m^2/°K^4).
T_s: is the water surface temperature (°C).
$\alpha_{\circ}$: is a proportionality constant (0.937E-5).

3.4.4 Evaporation

Evaporation flux is the flux resulting from the evaporation process known for all as "the process by which liquid water enters the atmosphere as water vapor. It is an important part of the exchange of energy in the Earth-atmosphere system that produces atmospheric motion and therefore weather and climate. The rate of evaporation depends on the temperature difference between the evaporating surface and the air, the relative humidity, and wind" (Augustyn & Rafferty, 2009). The value of evaporation falls in the range (0-35) Watt/m^2. Evaporation heat flux was obtained as follows (Cole & Wells, 2006):

$$H_e = f(W)(e_s - e_a) \quad \ldots\ldots\ldots\ldots\ldots (3-5)$$

Where
$f(W)$: wind speed function (Watt/m^2/ mmHg)

W: measured wind speed at a certain height above the water surface (m/sec).

e_s: saturated vapor pressure at T_s (mmHg).

e_a : atmospheric vapor pressure at $2m$ above the water surface (mmHg).

Saturated vapor pressure is a mathematical trend of the surface water temperature. It can be computed based on relative humidity (R_h):

$$e_s = 4.596\, EXP\left(\frac{17.27T_s}{(T_s + 273.3)}\right) \ldots\ldots\ldots\ldots\ldots (3-6)$$

And the air vapor pressure depends on both ambient air temperature and air relative humidity.

$$e_a = R_h e_s \ldots\ldots\ldots\ldots\ldots (3-7)$$

Air vapor pressure is computed based on dew point temperature:

$$e_a = 4.596 EXP\left(\frac{17.27T_d}{T_d + 273.3}\right) \ldots\ldots\ldots\ldots\ldots (3-8)$$

T_d: Dew point temperature (°C).

3.4.5 Conduction

Conduction is the process of heat swap between direct contact masses that have different temperatures. The process is happening at the air-water border and can be settled out using the resulting equation from the Bowen ratio (Cole & Wells, 2006; Kalinowska, 2019):

$$H_c = C_c f(W)(e_s - e_a) \ldots\ldots\ldots\ldots\ldots (3-9)$$

Where C_c is Bowen's coefficient (0.47 mmHg/ °C).

Conduction heat flux values are (-70 - 200) Watt/m^2 (Al-Zubaidi, 2018). It can cool down or warm up the water temperature, and this happens when the air

temperature is less or greater than the water temperature, respectively (Edinger & Geyer, 1974).

3.5 Wind Speed Function

The wind speed function is commonly a linear and sometimes quadratic function of wind speed and may be written as (Cole & Wells, 2006) :

$$f(W) = a + bW^c \quad \ldots\ldots\ldots\ldots\ldots (3-10)$$

Where a, b, $and\ c$ are empirical coefficients. Values of a, b, and c were taken as suggested:

a = 9.4 Watt /m^2/ mmHg.

b = 0.46 Watt /m^2/ mmHg/(m/sec)^2.

c = 2.

For rivers, it should be measured typically 2 meters above the surface. (sometimes 1.5 m), and for lakes and reservoirs, it is usually measured at 7, 8 or 10 meters above the surface (Monika Barbara Kalinowska, 2019). Other researchers suggested the wind speed, for any waterbody, should be measured at 2 m above the water surface (Al-Zubaidi, 2018; Shanahan, 1984). The wind speed generally increases with the height. Wind speed needs to be set to a certain height based on Ryan and Harleman (1973):

$$\frac{W_z}{W_{z1}} = \frac{ln\,(\frac{Z}{Z_\circ})}{ln\,(\frac{Z_1}{Z_\circ})} \quad \ldots\ldots\ldots\ldots\ldots (3-12)$$

Where

W_z: the desired wind velocity (m/sec) at elevation z (m).

W_{z1}: the known wind velocity (m/sec) at elevation z1. (m).

$Z_\circ$: the wind roughness height (m).

Z: height of desired wind velocity (m).

Z_1: height of known wind velocity (m).

In addition, a wind sheltering coefficient, WSC, is advised to correct the wind speed at the measuring location to the waterbody surface location. The correction style was as a multiplication factor to wind speed (Cole & Wells, 2006).

CHAPTER FOUR

Results and Discussion

4.1 Surface heat flux budget model simulation

To show the results, the simulation time was divided into several sections to reveal the fluctuations and reactions to the variations of fluxes during different durations. The whole data simulation period is (487-670) Julian Day. Many researchers contend that short-wave radiation owns its maximum strength on summer days (Lofgren & Zhu, 2000). In this work, the maximum value for the solar radiation was 842 Watt/m^2 at 540 Jday. It is a typical value for the summer day's season. This is shown in Fig. (4-1). The peaks for atmospheric radiation was around 454 Watt/m^2 at 635 Jday. The atmospheric peak is smaller than the solar radiation, but it still hits the maximum on the summer days. The reason behind that atmospheric flux depends on the air temperature. When the solar rays hit their maximum in the summer and rise the air temperature, it becomes very normal for the atmospheric radiation to have a rise in those days , see Figure (4-2).

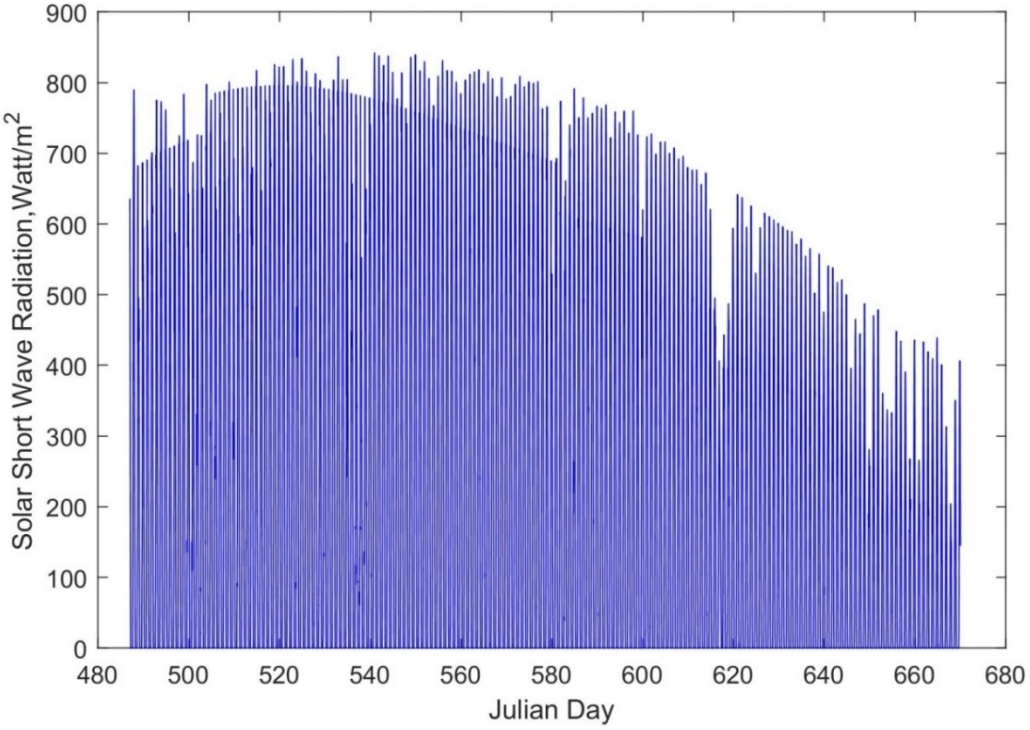

Figure (4-1): Short wave radiation flux.

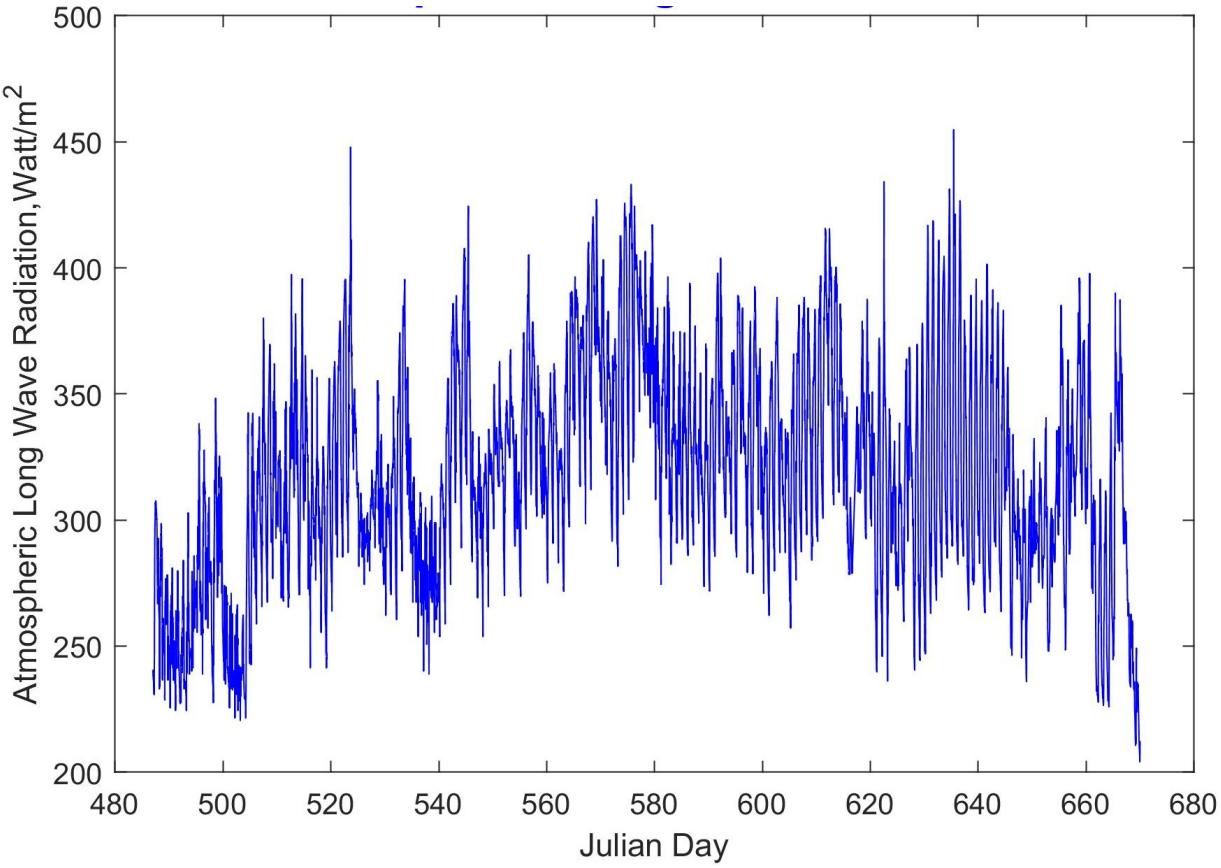

Figure (4-2): Atmospheric long-wave radiation fluxes.

In contrast to atmospheric radiation, long-wave back radiation depends primarily on water surface temperature. It strikes its maximum value on hot days as a result of the water is being affected by solar radiation and atmospheric radiation (Fig. (4-3)). Back radiation has 410 Watt/m^2 at 576 Jday as a maximum value.

When evaporation remarked a maximum value of 359 Watt/m^2 at 578 Jday, conduction has 169 Watt/m^2 as the highest value on the same day. The aforesaid is applied for the deepest falling, evaporation takes -66 Watt/m^2 as the minimum value at 659 Jday and conduction has on the same day -31 Watt/m^2 as a lowest value. Figures (4-4) and (4-5) reveal the linking relationship between evaporation and conduction heat fluxes. Finally, the total heat flux recorded

770.7631 Watt/m^2 as a maximum value at 508 Jday, and this is normal for sunny summer days. For winter days, its values surely will dropdown. This dropdown happened as its minimum value recoded -448.92 Watt/m^2 at 578 Jday (Fig. (4-6)).

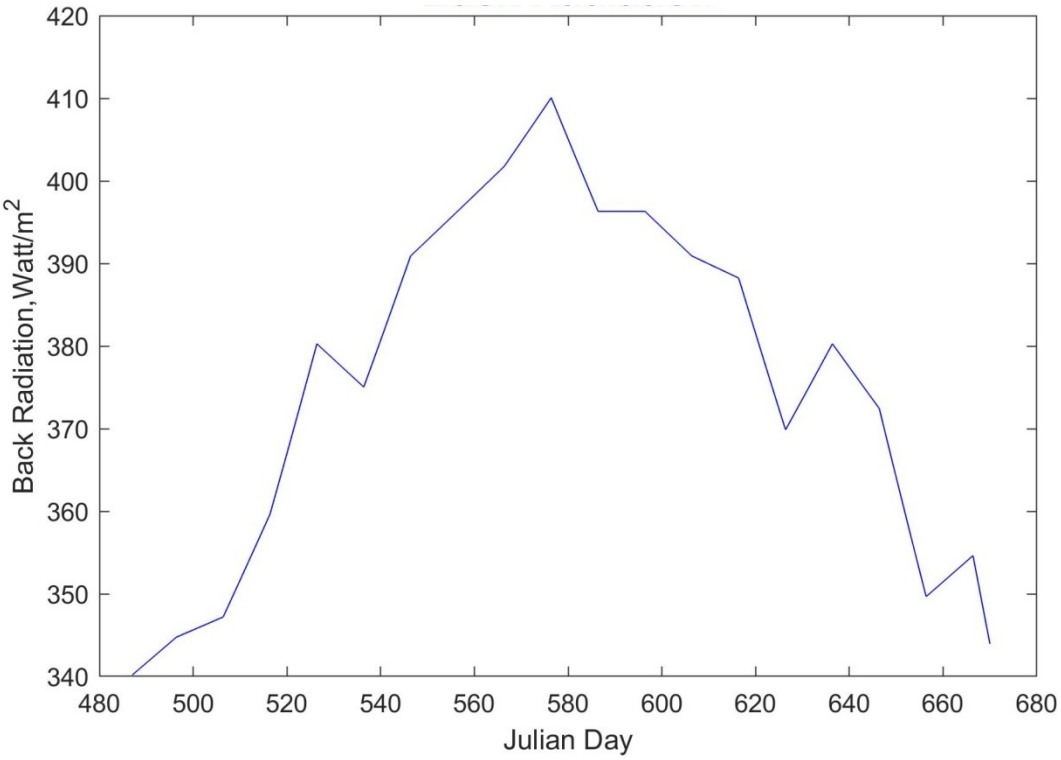

Figure (4-3): Back long-wave radiation fluxes.

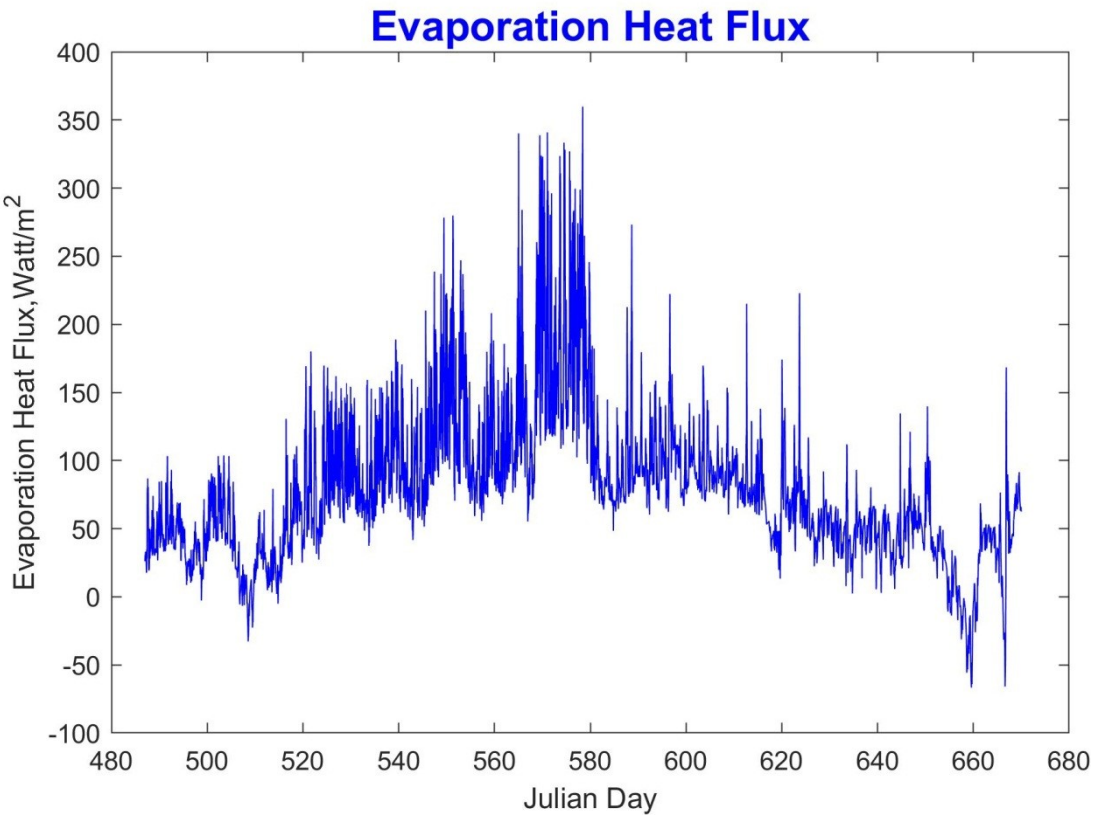

Figure (4-4): Evaporation fluxes.

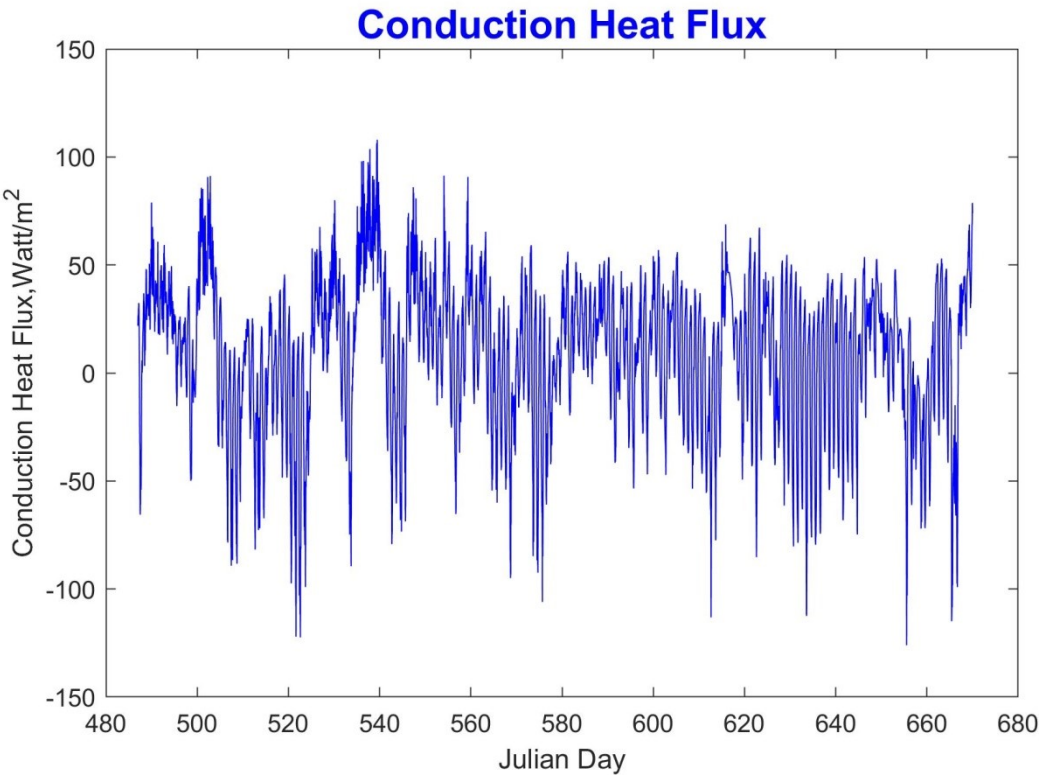

Figure (4-5): Conduction fluxes.

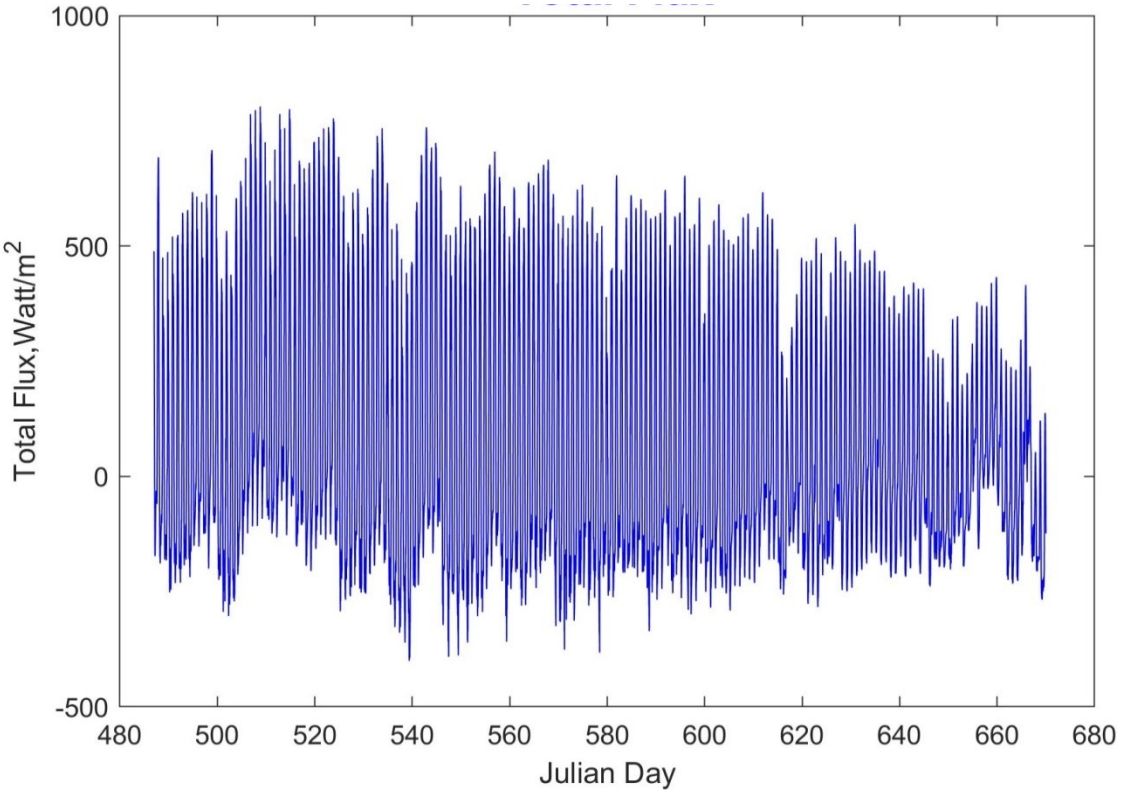

Figure (4-6): Total heat fluxes.

Several periods of time (515-545), (576-606), and (638-668) Julian day was chosen (Fig. (4-7)) in which the solar radiation impact on total flux appears clearly. The total heat flux behaves similar to the solar radiation flux. This proves that the major effect on the total heat budget is related to the solar radiation. Solar radiation has 287, 249 and 113 Watt/m^2 as a mean value for (515-545), (576-606), and (638-668) Julian day, respectively. It was noted that the solar radiation mean values went down referring to the winter season. The same happened to the total flux where its mean values dropped from 100 Watt/m^2 at (515-545) to 25 Watt/m^2 at (576-606) and reached 11 Watt/m^2 at (638-668). Table (4-1) shows the mean values of the atmospheric, back radiation, evaporation and conduction heat fluxes.

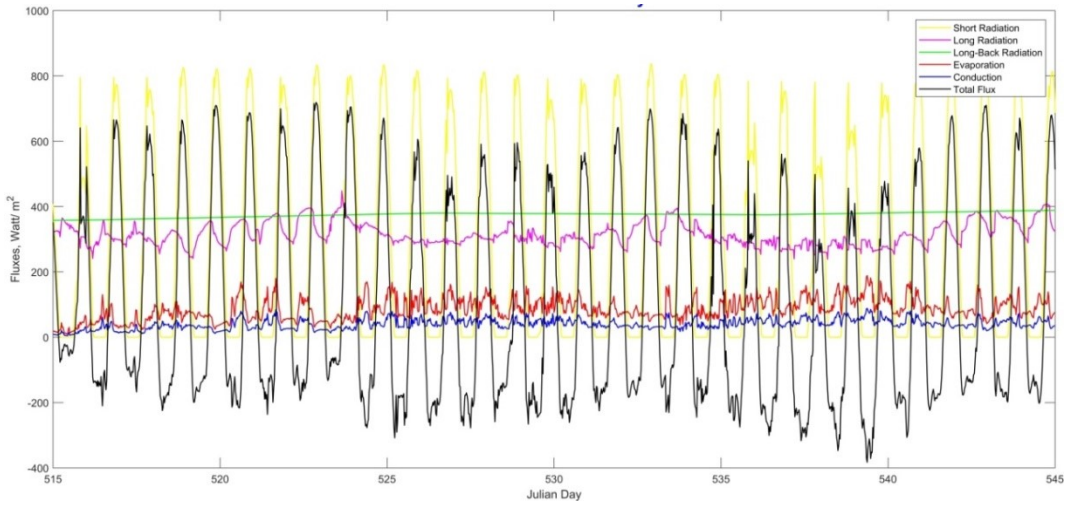

(a)

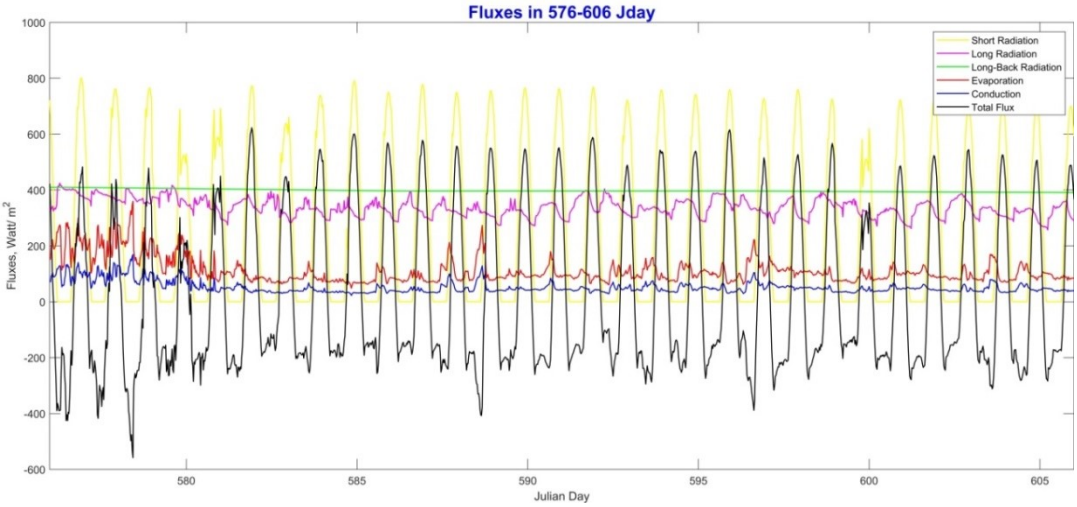

(b)

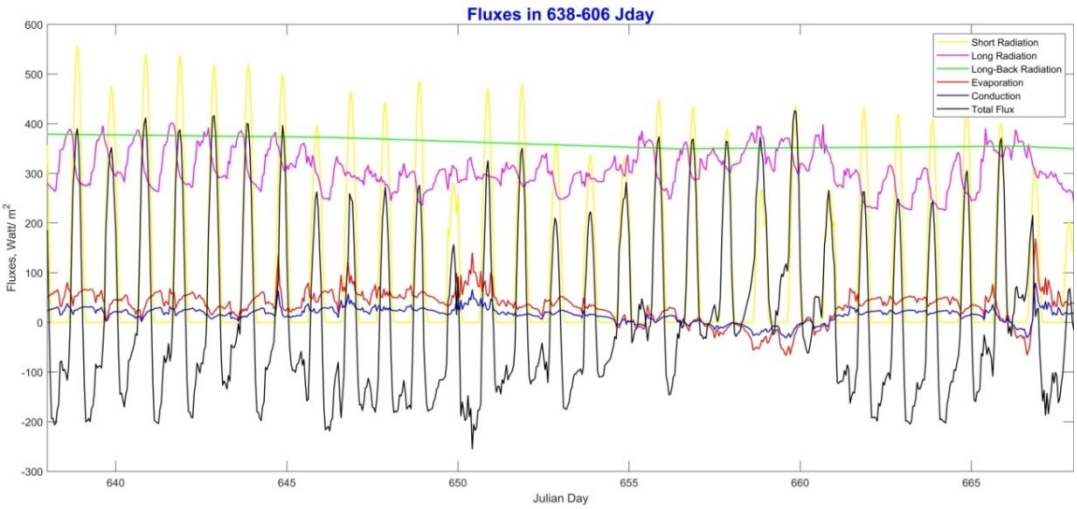

(c)

Figure (4-7): Fluxes at (a): 515-545, (b). 576-606, and (c): 638-668 Jday**.**

Table (4-1): The mean values for (515-545), (576-606) and (638-668) Jday.

Fluxes Watt/m^2	515-545	576-606	638-668
Atmospheric radiation	314	337	307
Back radiation	375	397	361
Evaporation	85	111	32
Conduction	40	52	15

For more details about the fluxes behavior, several weekly periods were chosen with a selected day. The periods were (500-507), (550-557), and (590-597) Julian days (Fig. (4-8)). Solar radiation strongly showed its control effect on the total radiation. In every solar radiation top and bottom peak, total flux follows these with a different scale. Also, solar radiation appears to fluctuate between zeros at night hours and reaches gradually the maximum intensity at midday. Solar radiation comes in two cycles. The first one is the daily cycle caused by the rotation of the earth around itself. The other cycle is the annual cycle caused by the rotation of the earth around the sun.

Atmospheric radiation has been remaining under the effect of the air temperature. Air temperature, in turn, is affected by solar intensity. On the other hand, back radiation has a steady behavior, but it has a slight gradient. The twinning of evaporation and conduction appears clearly. Every rise and drop in evaporation flux, conduction continued up with. Table (4-2) summarizes the minimum values for atmospheric radiation, back radiation, evaporation, conduction, and total heat flux.

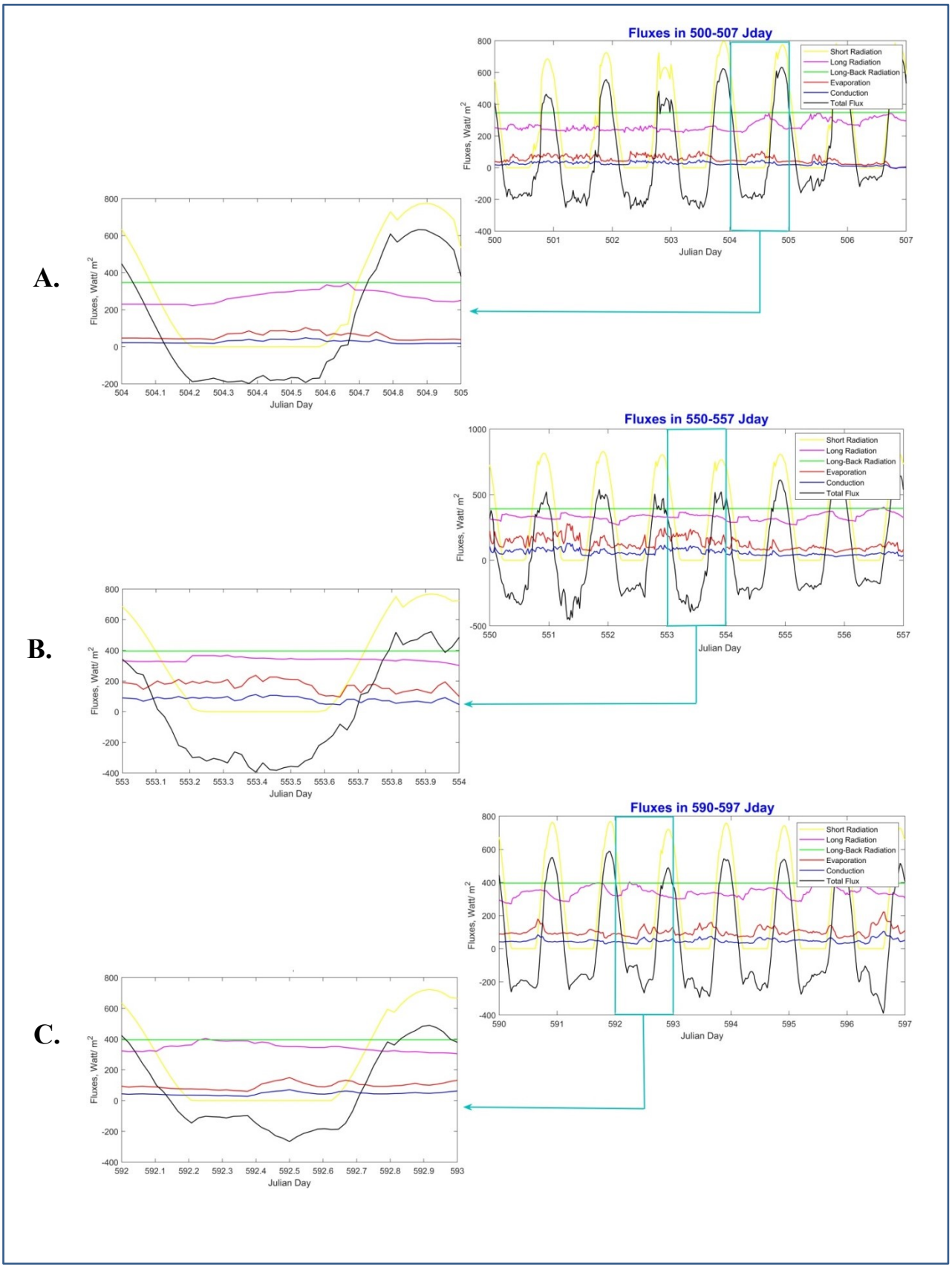

Figure (4-8): Fluxes for A. (500-507), B. (550-557), and C. (590-597) Jday.

Table (4-2): The minimum values summarization for atmospheric radiation, back radiation, Evaporation, conduction, and total flux.

Fluxes Watt/m^2	500-507	504-505	550-557	553-554	590-597	592-593
Atmospheric radiation	220	221	269	301	271	304
Back radiation	345	346	392	394	395	396
Evaporation	-5	35	59	94	60	60
Conduction	-2	16	27	44	28	28
Total flux	-260	-198	-455	-394	-388	-266

4.2 Model sensitivity:

4.2.1 Wind sheltering coefficient (WSC)

The model development accounts for the lake sensitivity to wind shielding. The total shear force on the water surface is related to a wind sheltering coefficient and the wind-affected lake area. To correct the wind speed, it was suggested to multiply wind speed by a wind sheltering coefficient (WSC) (Cole & Wells, 2017). When WSC is equal to 1, this means no corrections are needed (Al-Zubaidi, 2018). To study this effect, (0-2) range of values for WSC was chosen, and it is applied for three periods ((487-670) Jday, (490-497) Jday, and (492-492.5) Jday) as shown in Fig. (4-9), (4-10), and (4-11).

To show the effect of WSC on the total heat flux, a comparison was made between the average total fluxes for each WSC as shown in Table (4-1). WSC affects both evaporation and conduction, which are responsible for lowering the total heat flux. This leads to conclude that when WSC is low, the average total flux becomes higher. When WSC = 0, which is the lowest value,

the average total heat flux recorded a high value of 184.709 Watt/m^2. Also, the average total flux registered -65.319 Watt/m^2, which is the lowest value with a comparison of 184.709 Watt/ m^2, when WSC=2.

Table (4-3): Mean values of total heat flux for every WSC value.

WSC	***Mean Total Flux Watt/ m^2***	***WSC***	***Mean Total Flux Watt/ m^2***
0	184.709	**1.2**	34.692
0.2	159.706	**1.4**	9.689
0.4	134.703	**1.6**	-15.313
0.6	109.700	**1.8**	-40.316
0.8	84.697	**2**	-65.319

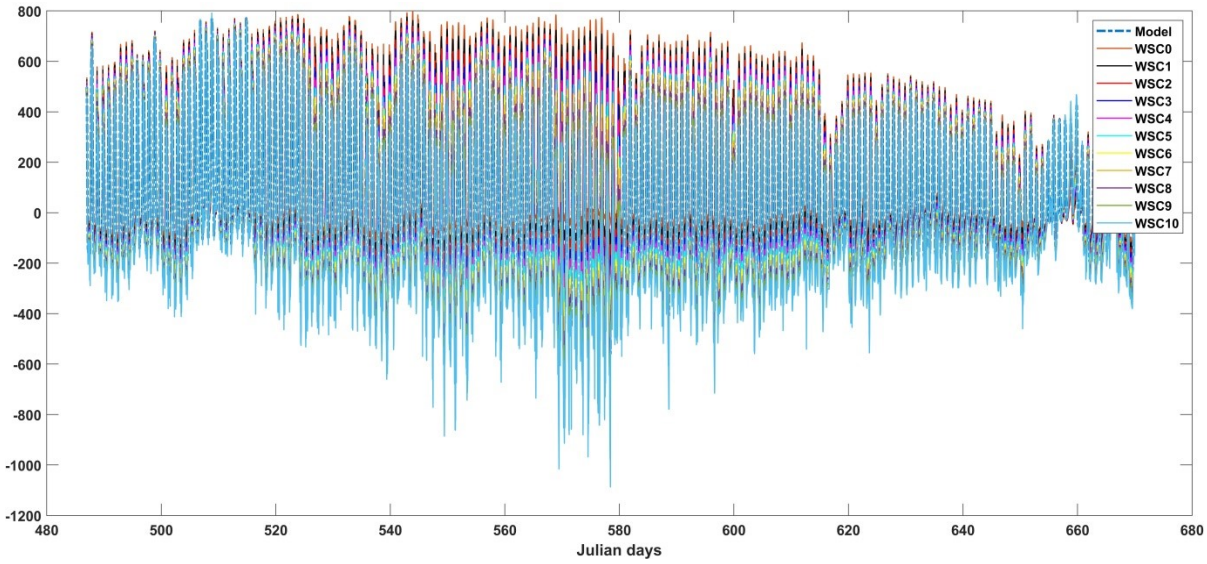

Figure (4-9): WSC effects for (487-670) Jday.

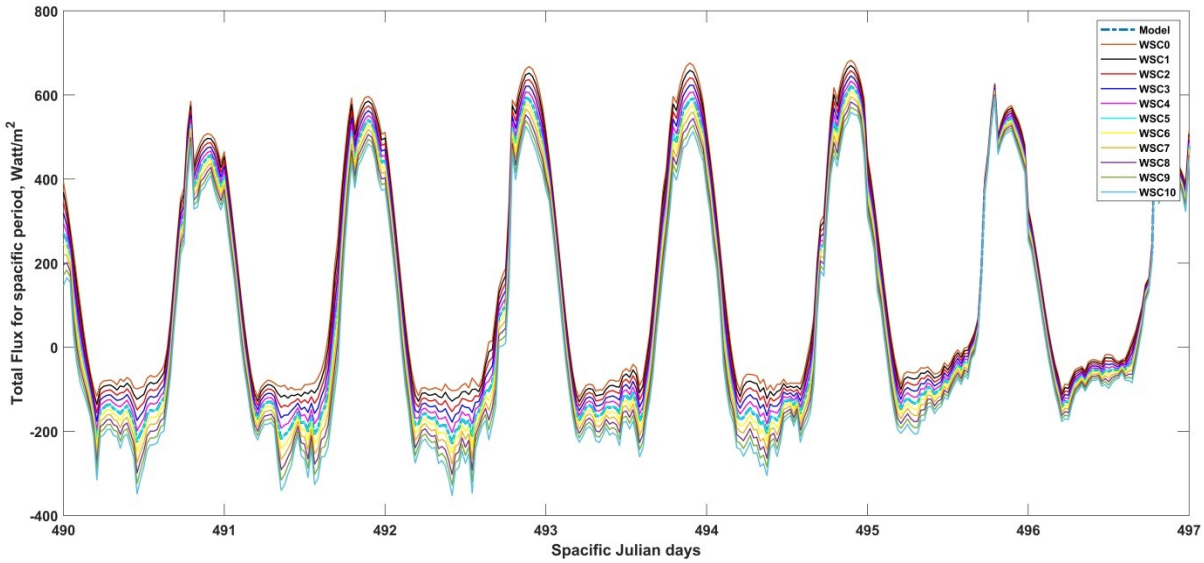

Figure (4-10): WSC effect for (490-497) Jday.

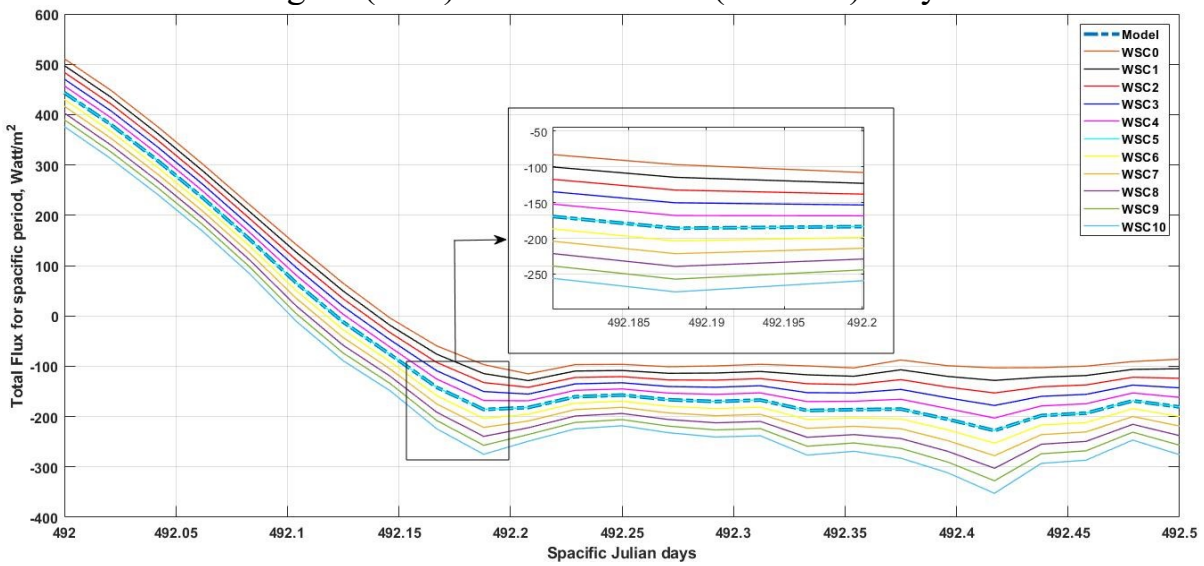

Figure (4-11): WSC effect for (492-492.5) Jday.

4.2.2 Model Sensitivity of wind speed function to Edinger-wind coefficients

Calibration was made for wind coefficients suggested by Edinger, where several ranges for coefficients were assumed to examine the changes in the total flux. Certainly, to show the consequences of these changes, Julian day periods of (532-532.5) and (487- 670) were selected.

To study the coefficient "a " effect for calibration purposes, a domain of (9-10) was adopted as shown in Fig. (4-12) and (4-13). In these Figures, the model and the "A4" hold the same values of "a". The highest value of total flux was 775.061 Watt/m^2 when a=10. While for a = 9 the maximum total flux was 773.649 Watt/m^2, the model scored the highest total flux at 774.214 Watt/m^2.

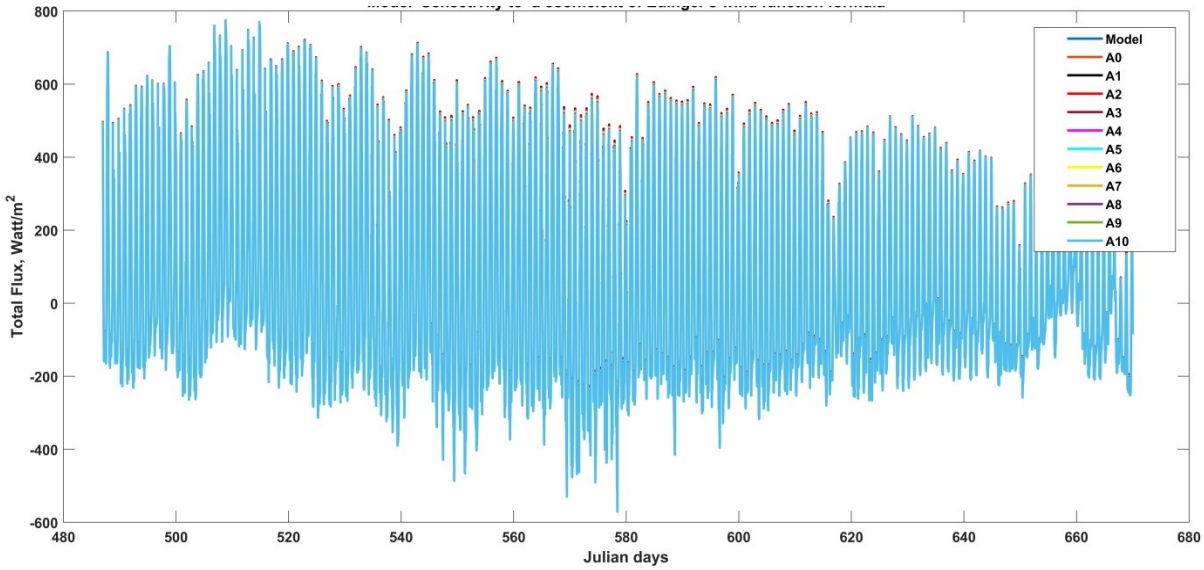

Figure (4-12): Model sensitivity to Edinger wind speed function coefficient "a".

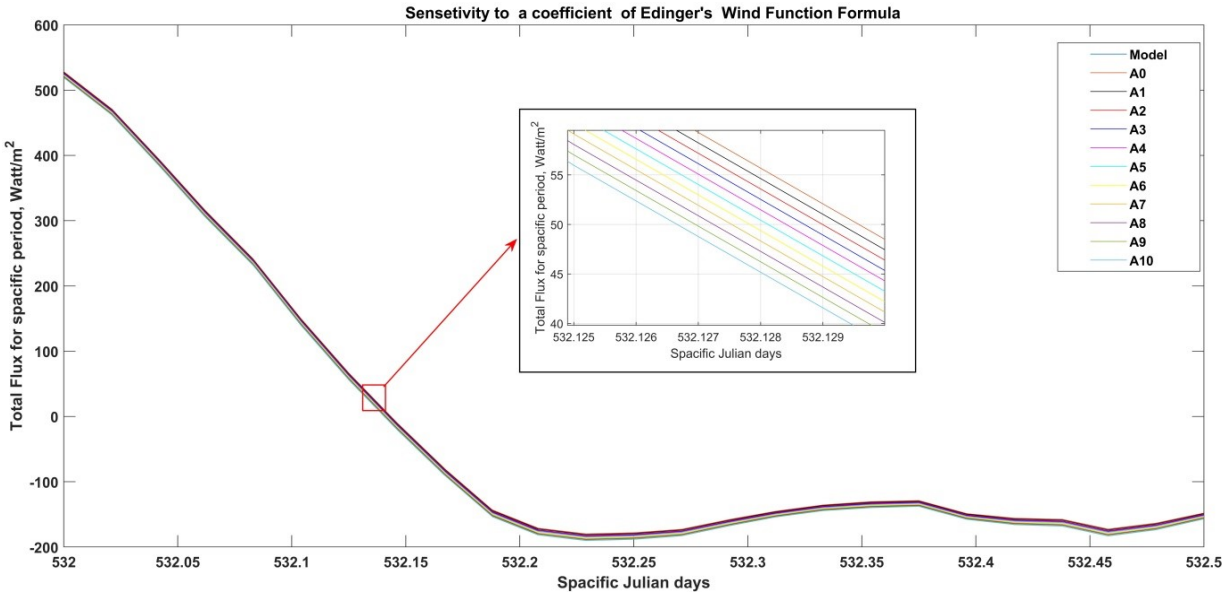

Figure (4-13): Model sensitivity to Edinger wind speed function coefficient "a" for (532-532.5) Jday.

The calibration of coefficient "b" was in between (0-1) as appeared in Fig. (4-14) and (4-15). For this range, the model displayed "B4" with (b4= 0.4) and "B5" with (b5= 0.5). The model "b" coefficient value of (0.46) highlighted clearly that. The highest-ranking value for total flux is 778.714 Watt/m^2 at b=1, while the maximum value at b= 0 was 770.380 Watt/m^2. The model total flux has a maximum value that goes between B4 (when b=0.4, 773.714 Watt/m^2) and B5 (when b=0.5, 774.547 Watt/m^2).

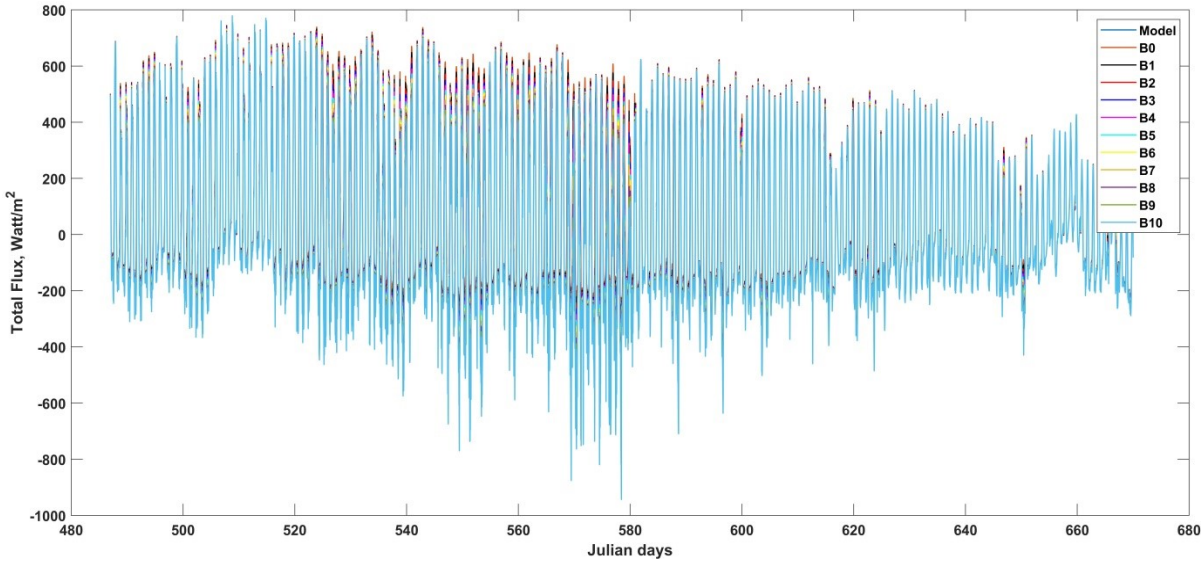

Figure (4-14): Model sensitivity to Edinger wind speed function coefficient "b".

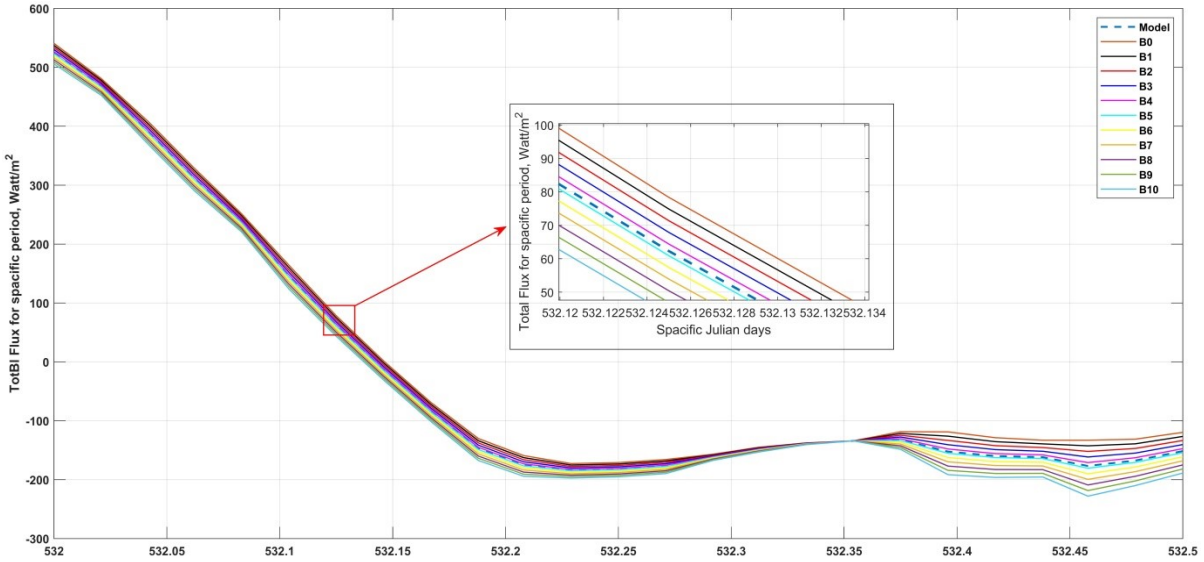

Figure (4-15): Model sensitivity to Edinger wind speed function coefficient "b" for (532-532.5) Jday.

For the coefficient "c", the range of calibration was (1-2). Again, the model united with one of the calibration lines because of their equal values as shown in Fig. (4-16) and (4-17). there is an evidence that it is the total flux maximum value for the model is identical for c= 2. When c=1, the peak value hits 770.38 Watt/m^2.

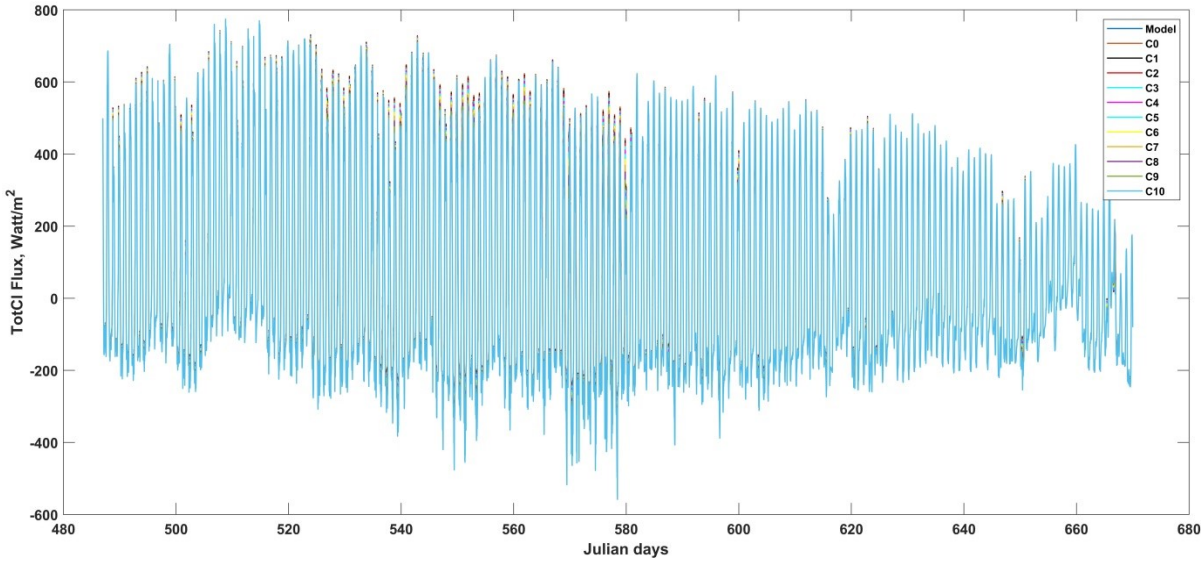

Figure (4-16): Model sensitivity to Edinger wind speed function coefficient "c".

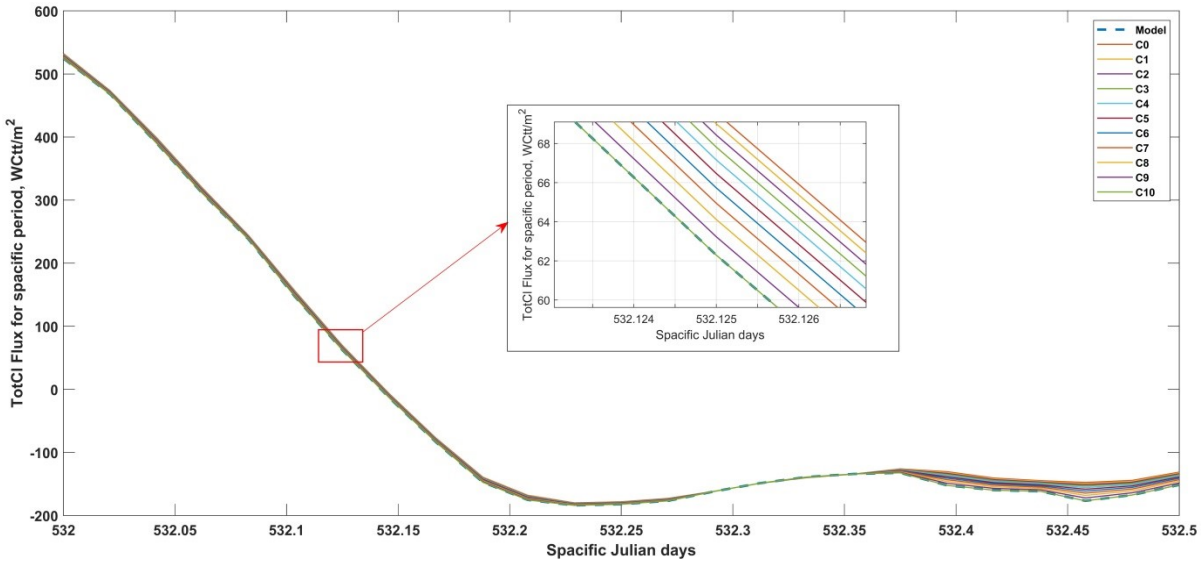

Figure (4-17): Model sensitivity to Edinger wind speed function coefficient "c" for (532-532.5) Jday.

4.2.3 Other wind speed function formulas

The model applies Edinger's suggestion for wind speed coefficients (b1 = 9.4, b2= 0 and b3 =0.46). For more flexibility, other suggested functions as mentioned in Table (4-4) were investigated (Kalinowska, 2019). Figure (4-18) shows all wind speed function formulas for approximately eight months. While Fig. (4-19) clears the formulas for (508-509) Julian day.

Table (4-4): Wind speed functions (Kalinowska, 2019).

Wind Speed Functions Formula	b_1 $[W\,.\,m^{-2}.mb]$	b_2 $[W\,.\,m^{-2}.mb]$	b_3 $[W\,.\,m^{-2}.mb]$	$F(W)= (b_1 + b_2 W + b_3 W^2)$
Ahsan & Blumberg (1999); Arifin et al. (2016); and Ji (2017)	6.9	0	0.34	$(6.9 + 0.34\,W^2)$
Miller and Street (1972)	7.42	0	0.49	$(7.42 + 0.49W^2)$
Czernuszenko (1990)	0	3.75	0	$(3.75W)$
Marciano & Harbeck (1952)	0	2.07	0	$(2.07W)$
Ryan (1973)	6.9	3.07	0	$(6.9 + 3.07W)$
Meyer (1928)	8.4	3.07	0	$(8.4 + 3.07W)$

Evaporation and conduction fluxes are affected by wind. Therefore, wind speed functions in its return will affect the total heat flux. The mean total flux calculated with the wind speed functions suggested by Czernuszenko, Ahsen, and Millar have a difference from the model mean total flux below 13 Watt/m^2, scored (97.067, 92.756, and 75.067) Watt/m^2, respectively. While the mean total fluxes calculated with the wind speed function suggested by Ryan, Meyer, and Marciano have a difference from the model mean total flux exceeded 35 Watt/m^2, resulted in (34.036, 48.129, 126.982) Watt/m^2, respectively.

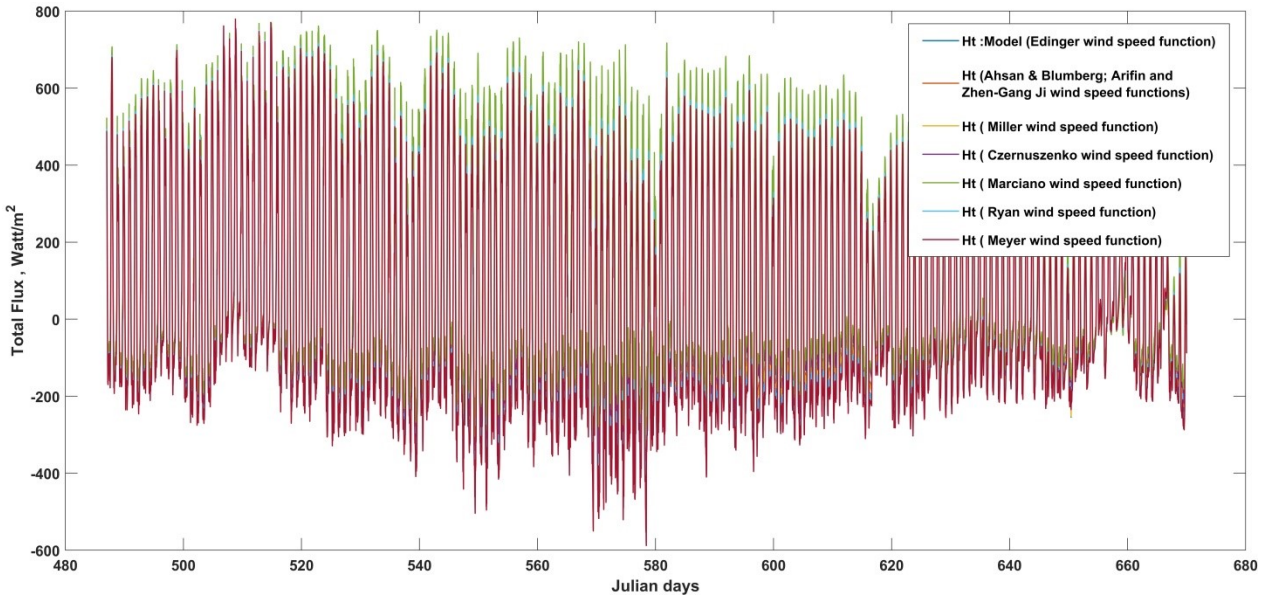

Figure (4-18): Wind speed function formulas effect.

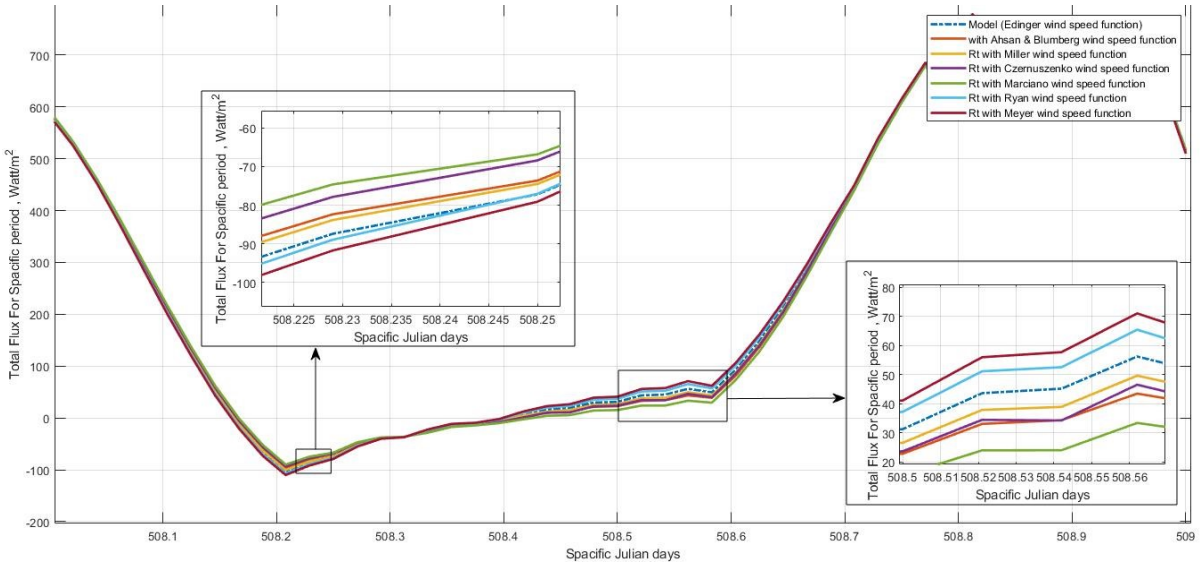

Figure (4-19): Wind speed function formulas effect for (508-509) Jday.

4.2.4 Model comparison of wind speed function formulas

To highlight the difference between Edinger's formula and other formulas, it was suggested to take the mean absolute error (MAE) and RMSE errors related to Edinger's formula. Table (4-5) abbreviated the value of each formula with its RMSE and MAE values. The highest recorded values for MAE and RMSE were 68.071 and 76.303, respectively for Marciano and Harbeck

formula. After that, Czernuszenko formula came with 37.910 and 46.090 as values of MAE and RMSE, respectively. While Ryan formula scored the lowest values (MAE of 13.851 and RMSE of 17.944).

Table (4-5): The MAE and RMSE values in (Watt/m^2) for each speed wind function.

Formulas	***MAE***	***RMSE***
Ahsan & Blumberg (1999); Arifin et al. (2016); and Ji (2017)	33.395	39.104
Miller and Street (1972)	16.411	18.375
Czernuszenko (1990)	37.910	46.090
Marciano & Harbeck (1952)	68.071	76.303
Ryan (1973)	13.851	17.944
Meyer (1928)	26.120	31.508

4.3 Air-water temperature modeling:

4.3.1 Sinusoidal-based model

The sinusoidal style was applied to this model to calculate water temperature. This style suggested that air temperature is a sinusoidal function of water temperature. Evaporation, conduction, and back radiation fluxes are going to be changed as it is a function of water temperature. This change will lead to different total heat flux. Sinusoidal style has recorded maximum long back-radiation of 405.075 Watt/m^2 at 575 Julian day. While long back-radiation of the model has been recorded a maximum value of 410 Watt/m^2 at 576 Julian day. Figure (4-20) shows the back radiation of both model and sinusoidal style. There is a gap of 20.588 Watt/m^2 between the mean value of evaporation flux from the model (85.048 Watt/m^2) and the sinusoidal style (64.46 Watt/m^2).

Evaporation flux by both the model and sinusoidal style is displayed in Fig. (4-21)

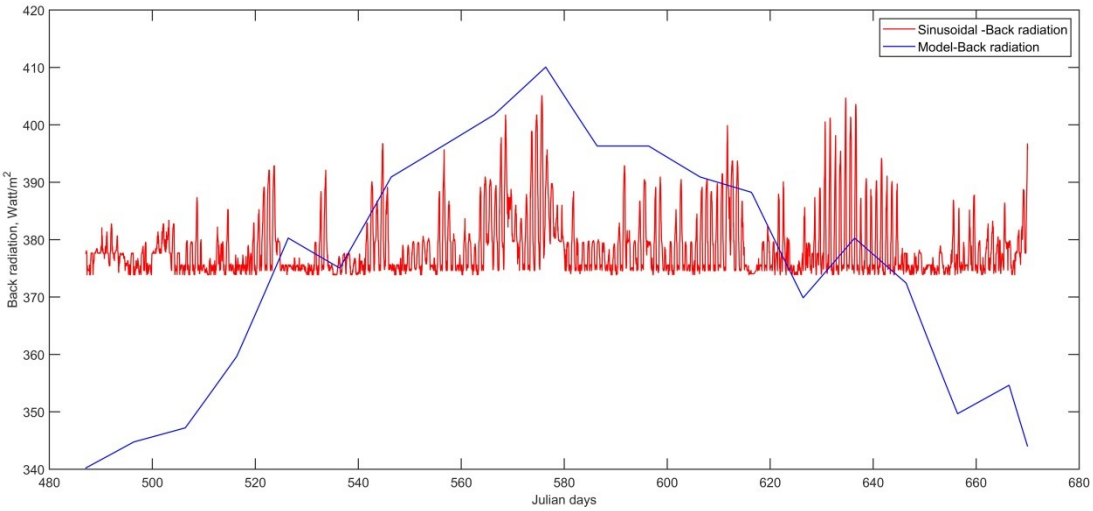

Figure (4-20): Back longwave radiation flux by the model and the sinusoidal style.

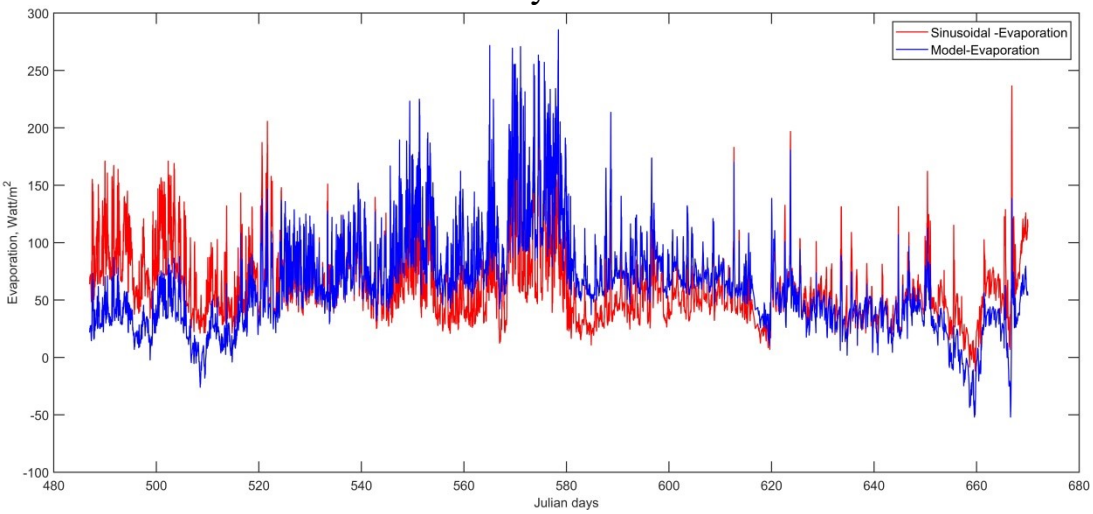

Figure (4-21): Evaporation flux by the model and the sinusoidal style.

For conduction flux, the model reports the minimum value of -24.4 Watt/m^2 at 659 Julian day, and the sinusoidal style shows a minimum of -115.86 Watt/m^2 at 575 Julian day. Figure (4-22) shows the conduction flux for the model and the sinusoidal style. At 575 Julian day, sinusoidal-based water temperature hits the maximum value of 20.6 celsius, and it is very close to the model maximum water temperature value of 21.5 Celsius at 576 Julian day. Figure (4-23) revealed water temperature for model and sinusoidal style modeling. A surpass of 15.812 Watt/m^2 between the maximum values of total

flux for the model and the style. Whereas style scored the peak at 790.026 Watt/m^2 at 542 Julian day, the model recorded 774.214 Watt/m^2 at 508 Julian day. Figures (4-24) and (4-25) show the total fluxes for the entire dataset and for one month, respectively.

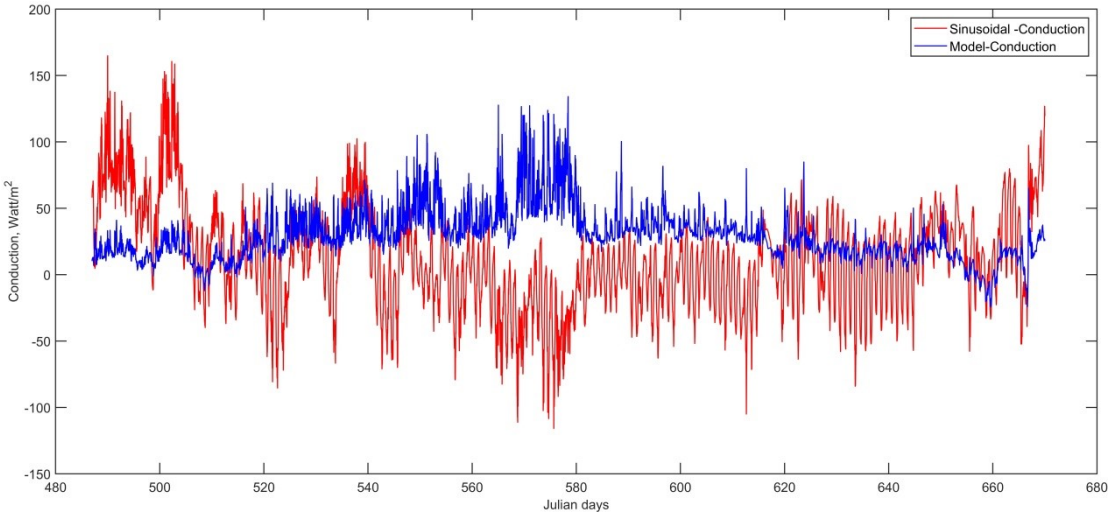

Figure (4-22): Conduction for the model and the sinusoidal style modeling.

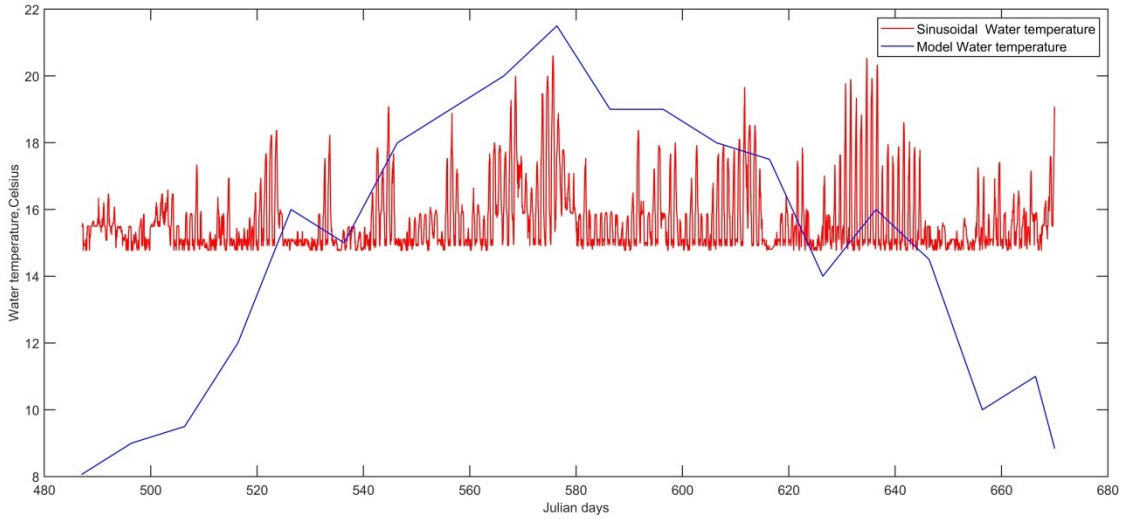

Figure (4-23): Water temperature for both model and sinusoidal style modeling.

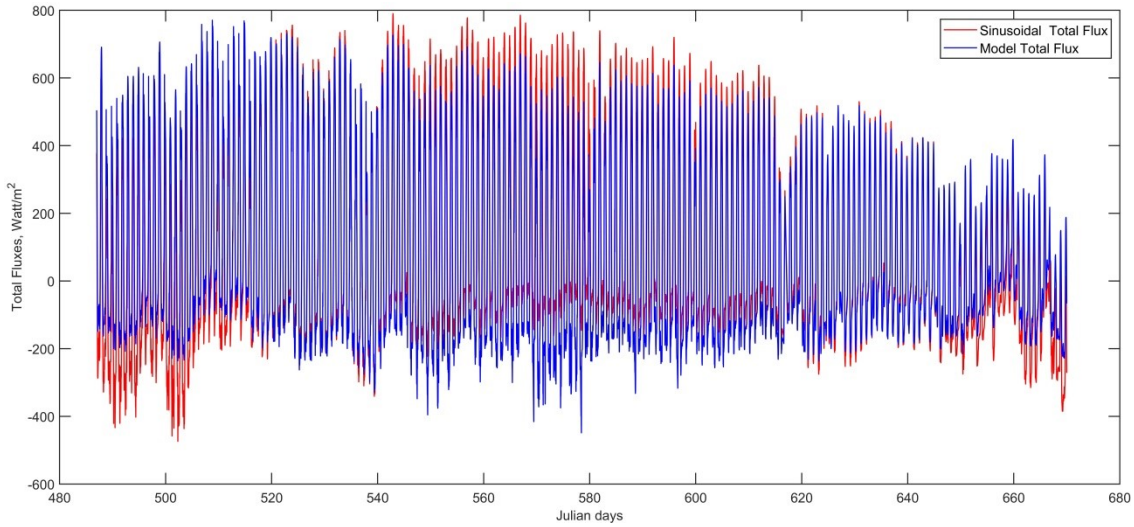

Figure (4-24): The total fluxes for the entire data range.

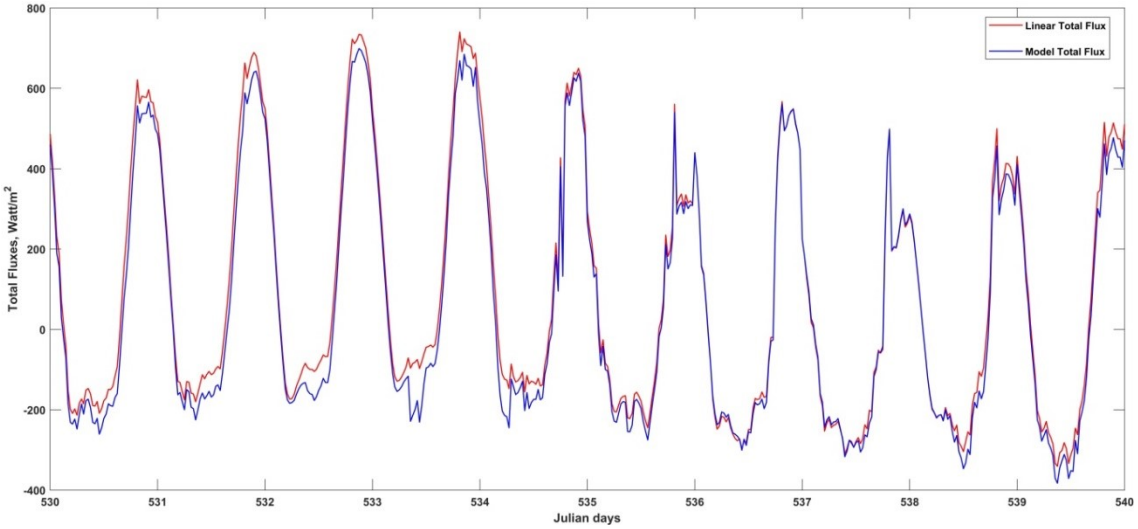

Figure (4-25): The total fluxes for (530-540) Jday.

4.3.2 Logistic-based model

Likewise, the sinusoidal model, logistic modeling will affect evaporation, conduction, and back radiation fluxes. These fluxes will affect the total flux as well. At 575 Julian day, logistic-back radiation hits the maximum value of 391.256 Watt/m^2, while the model maximum value is 410 Watt/m^2 on 576 Jday. Figure (4-26) shows the back radiation of model and logistic style. There is a gap of 19.251 Watt/m^2 between the mean value of evaporation of the model (85.048 Watt/m^2) and the logistic style (65.797 Watt/m^2). The evaporation of the model and logistic style are displayed in Fig. (4-27).

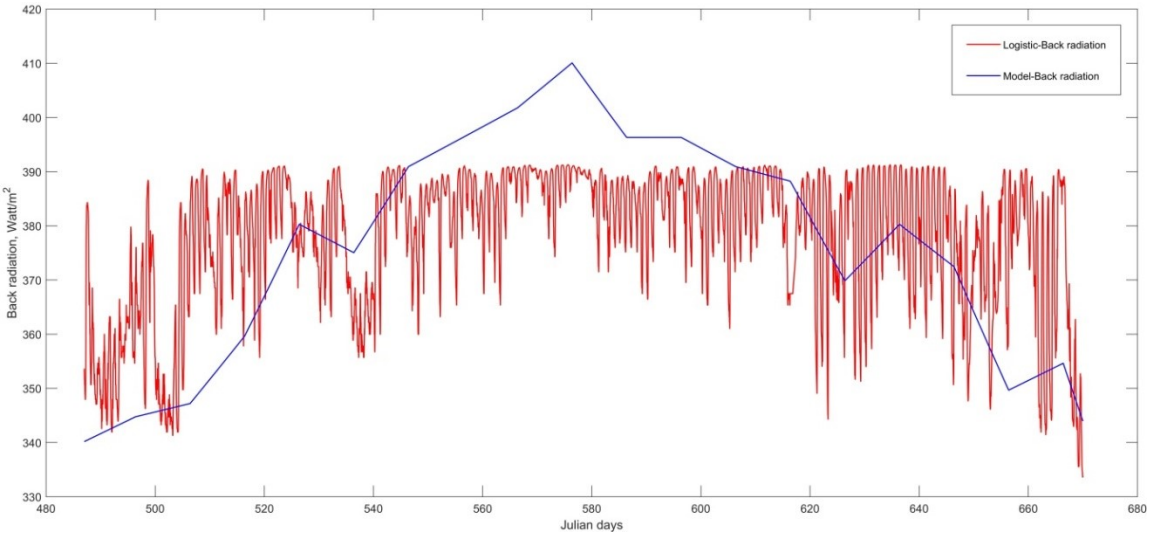

Figure (4-26): Back longwave radiation for the model and logistic style modeling.

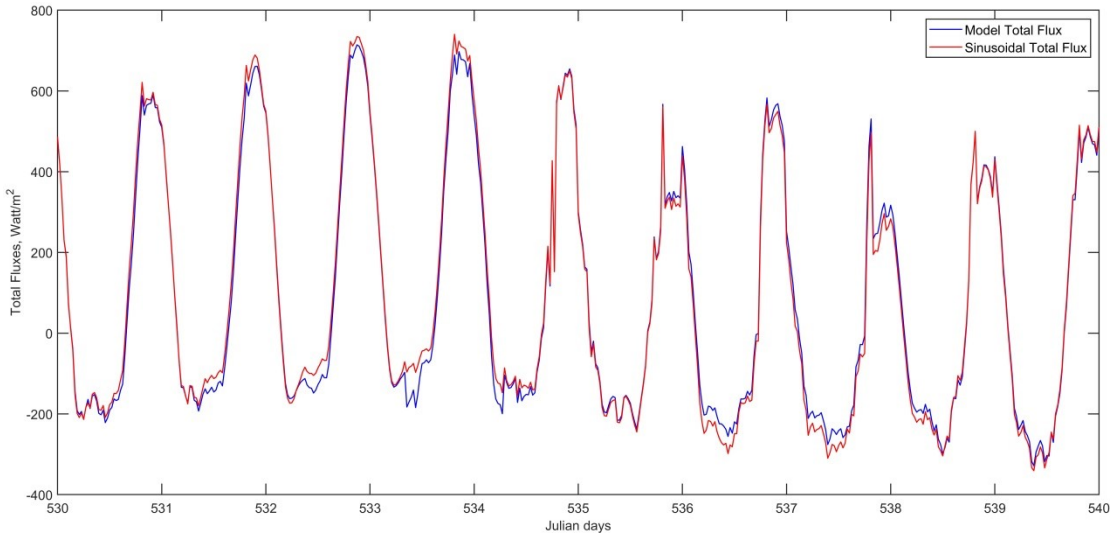

Figure (4-27): Evaporation for the model and the logistic style modeling.

The minimum conduction by logistic style was -142.664 Watt/m^2 at 575 Julian day, while minimum conduction by the model has been recorded -31.331 Watt/m^2 t 575 Julian day. Figure (4-28) shows the conduction of the model and logistic styles. The maximum water temperature by the logistic style was 18.064 celsius at 575 Julian day. While water temperature by the model has been recorded its maximum of 21.5 celsius at 576 Julian day. Figure (4-29) shows the water temperature of both the model and the logistic style.

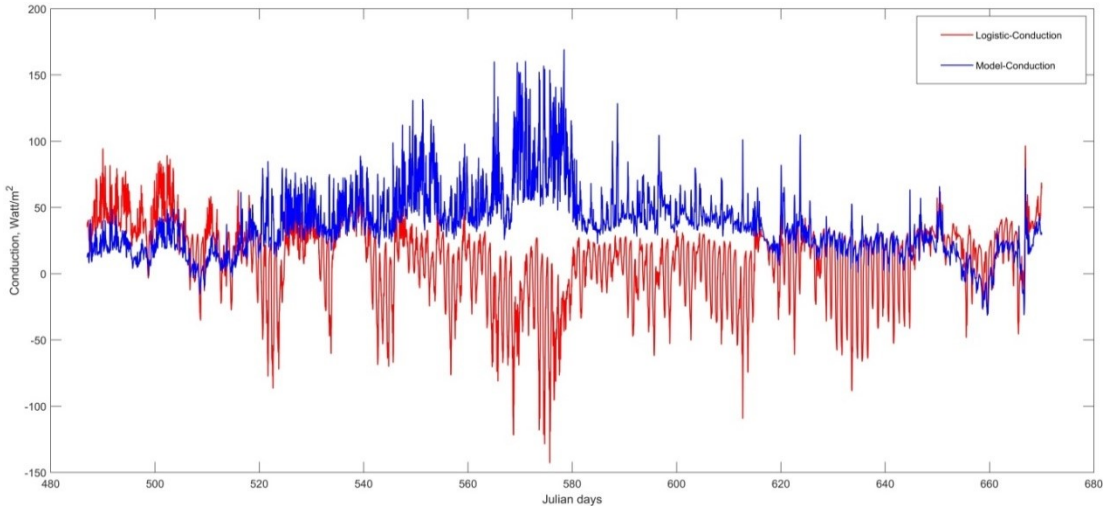

Figure (4-28): Conduction flux for the model and the logistic style modeling.

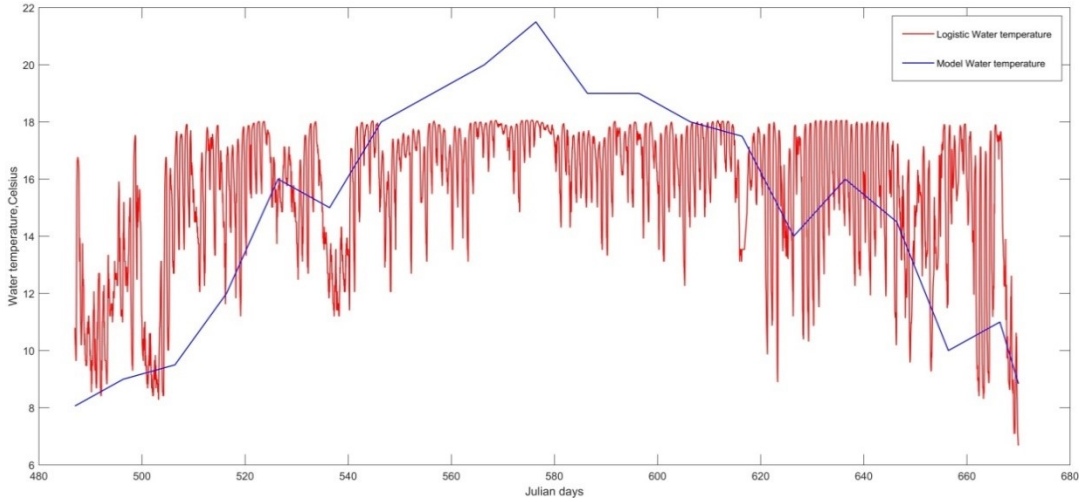

Figure (4-29): Water temperature for the model and the logistic style.

A gap of 21.693 Watt/m^2 between maximum values of the total flux for the model and this style. While the style marked a peak of 752.521 Watt/m^2 at 542 Julian day, the model hit 774.214 Watt/m^2 at 508 Julian day. Figures (4-30) and (4-31) showed the total fluxes for the entire data and for one month.

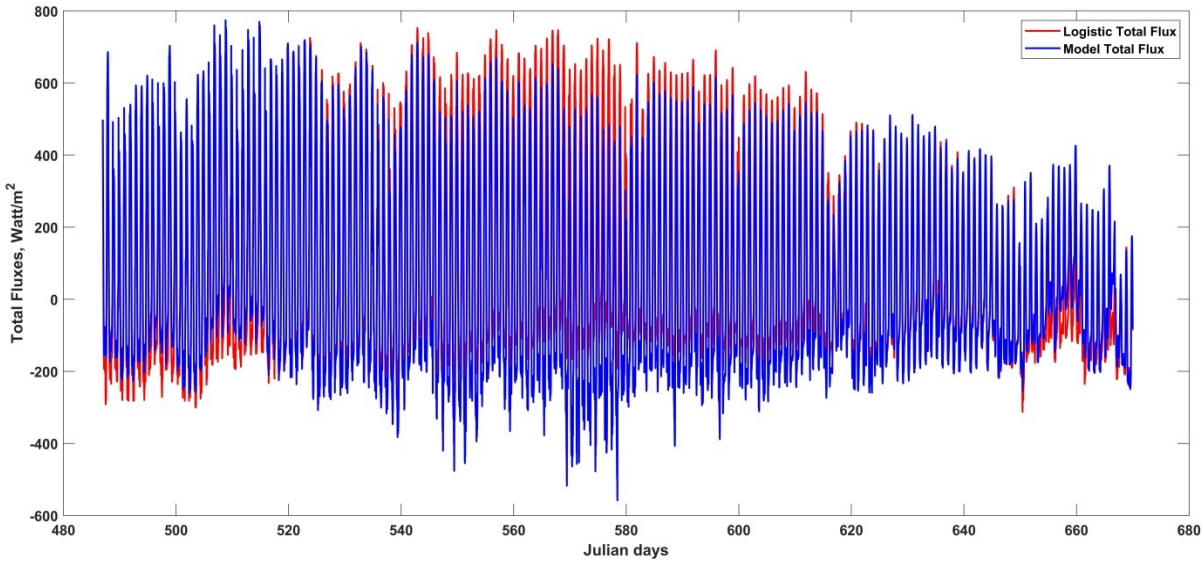

Figure (4-30): The total flux for the model and logistic style modeling for the entire data period.

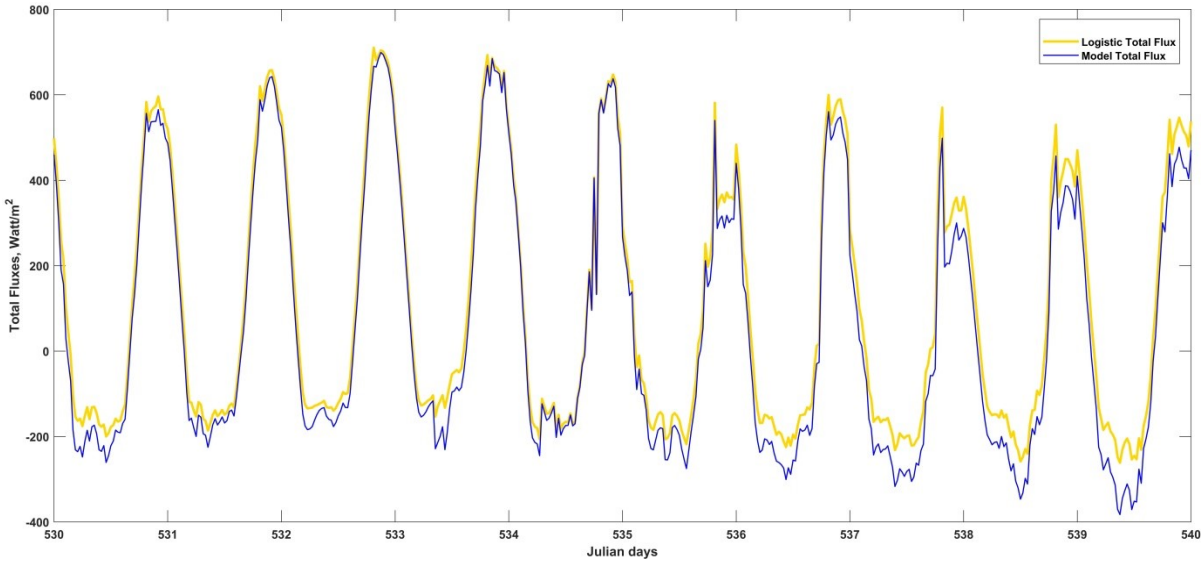

Figure (4-31): The total flux for the model and the logistic style modeling for (530-540) Jday.

4.3.3 Model comparison of water temperature with logistic and sinusoidal-based model

In order to show the difference between the total heat flux from the model, logistic, and sinusoidal style. MAE, RMSE, and Nash–Sutcliffe efficiency (NSE) errors were determined. Table (4-6) abbreviated the total flux values of each with its MAE, RMSE, and NSE values. In addition, Figures (4-32) to (4-

38) represent graphically the modeled fluxes of Table (4-6). A quick look at the Table is enough to realize several things: First, all the values of MAE and RMSE are growing except Nash–Sutcliffe efficiency (NSE) values which gradually went down then it increases during total period. Also, NSE at the period (560-562) and (560-563) were close, where the recordings of the two models are closer to the model at those periods. Furthermore, this approximately is applied to the period (560-564). After that, the two models record somewhat far away, besides the cumulative errors. Finally, the logistic style is more efficient than the sinusoidal style.

Table (4-6): MAE, RMSE, and NSE values for sinusoidal and logistic styles.

Range	***MAE***		***RMSE***		***NSE***	
	Logistic	*Sinusoidal*	*Logistic*	*Sinusoidal*	*Logistic*	*Sinusoidal*
560-561	0.470	0.614	5.949	7.953	0.944	0.901
560-562	0.931	1.275	8.369	11.692	0.941	0.886
560-563	1.404	1.916	10.285	14.345	0.942	0.885
560-564	1.957	2.546	12.467	16.481	0.938	0.892
560-567	4.1211	5.144	20.706	25.529	0.900	0.848
560-574	10.198	12.109	36.992	42.920	0.839	0.784
560-590	20.841	25.064	53.496	61.753	0.830	0.773
487-670	59.221	79.601	73.640	96.118	0.931	0.882

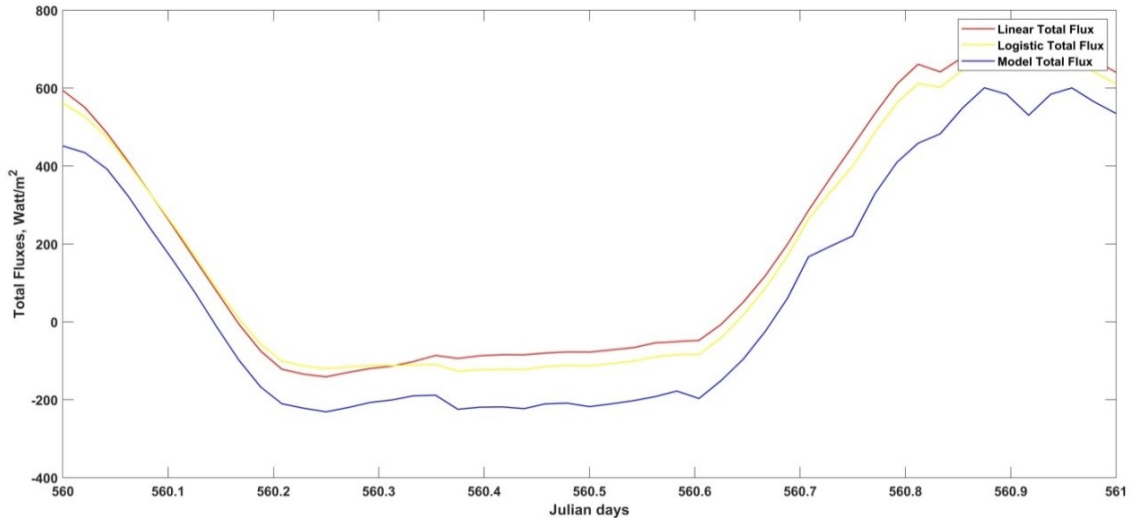

Figure (4-32): Model, logistic and sinusoidal styles for (560-561) Jday.

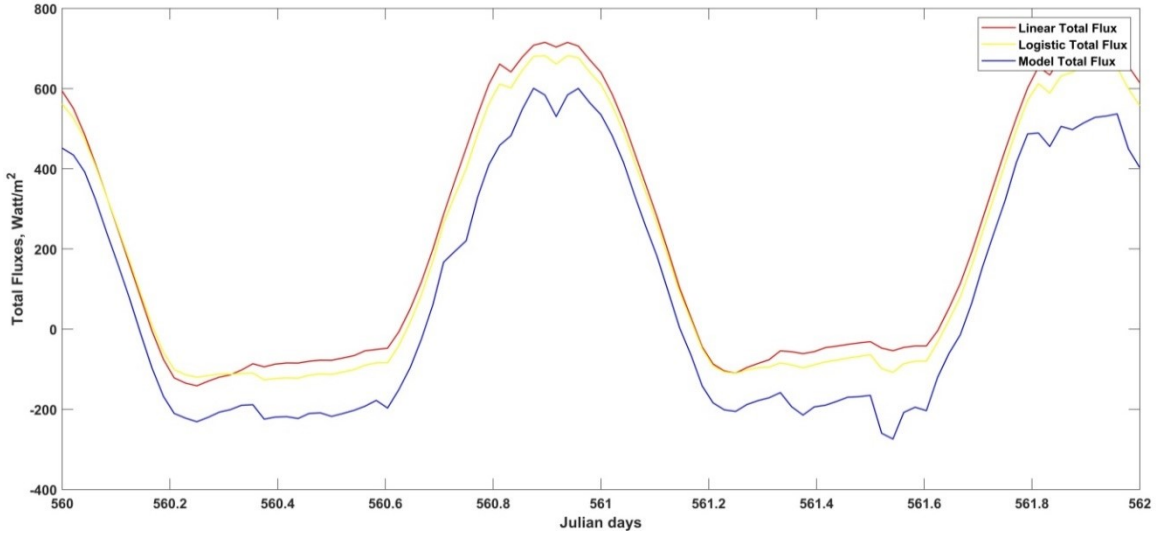

Figure (4-33): Model, logistic and sinusoidal styles for (560-562) Jday.

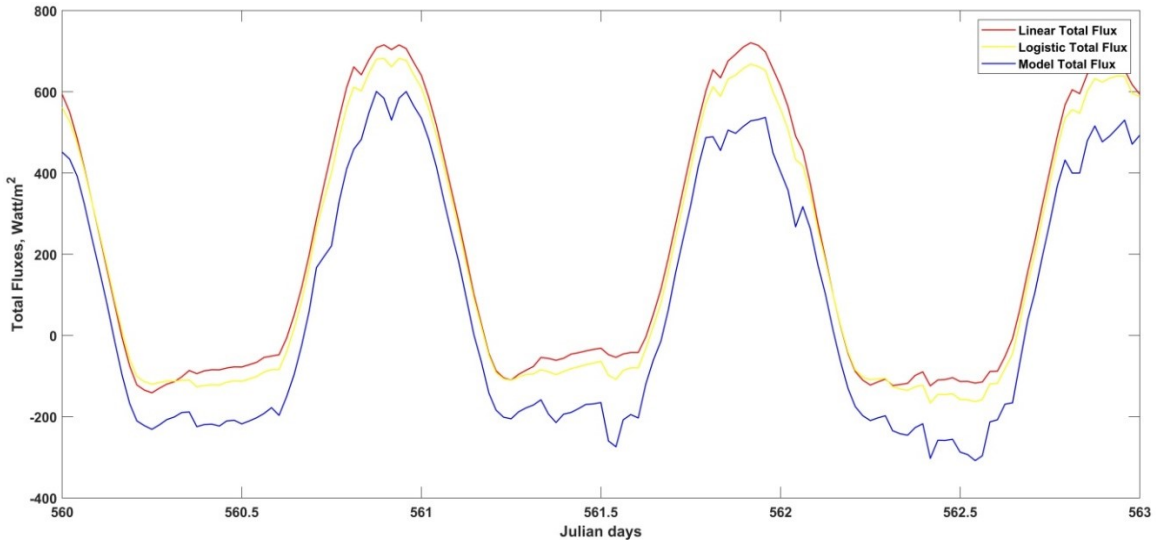

Figure (4-34): Model, logistic and sinusoidal styles for (560-563) Jday.

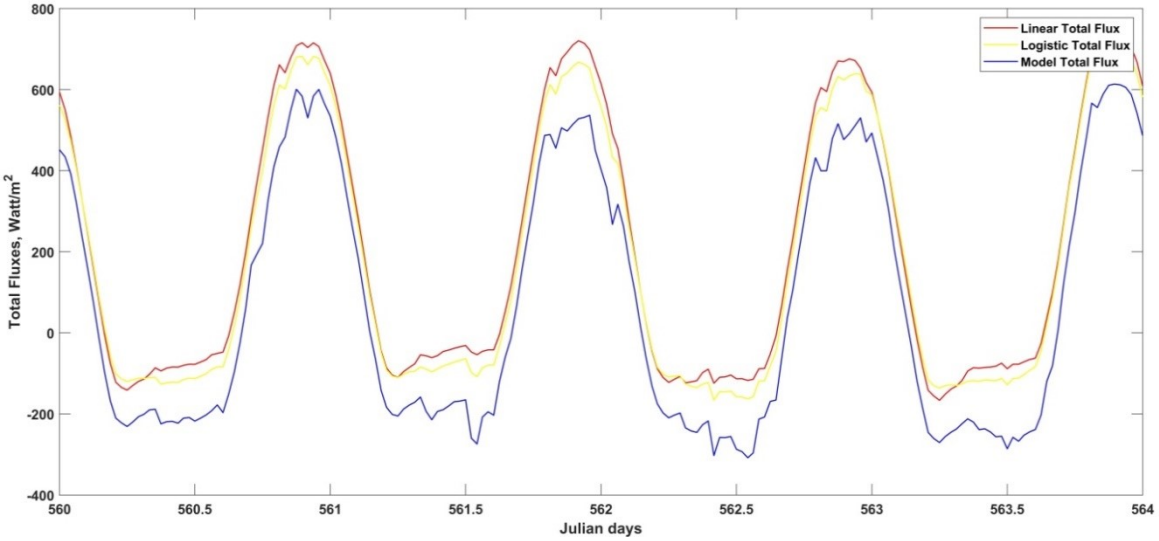

Figure (4-35): Model, logistic and sinusoidal styles for (560-564) Jday.

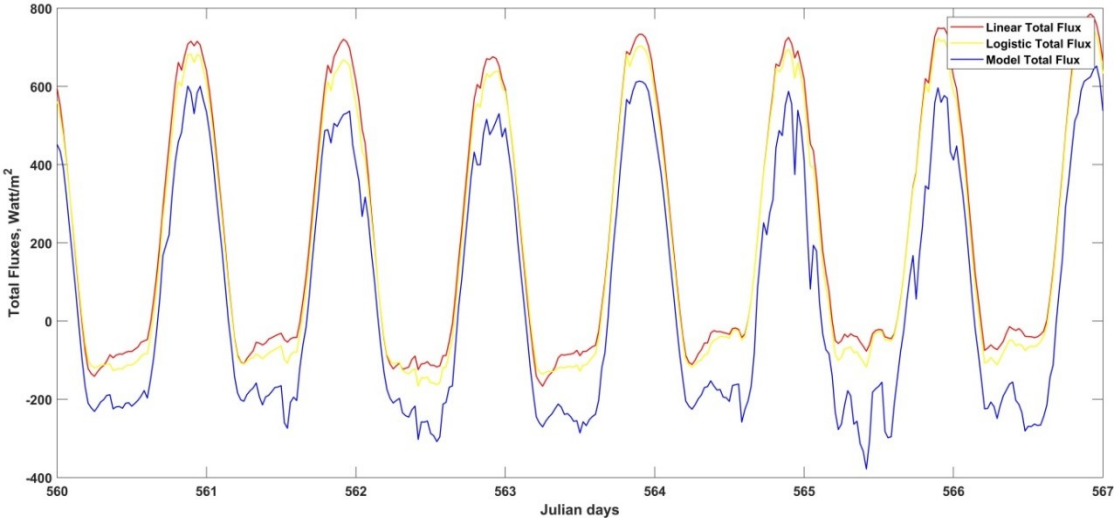

Figure (4-36): Model, logistic and sinusoidal styles for (560-567) Jday.

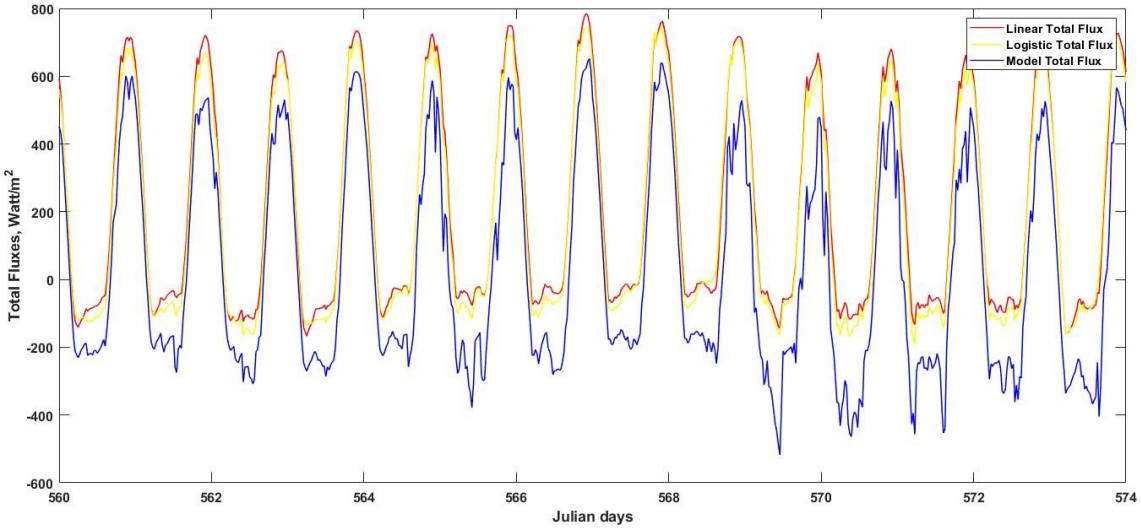

Figure (4-37): Model, logistic and sinusoidal styles for (560-574) Jday.

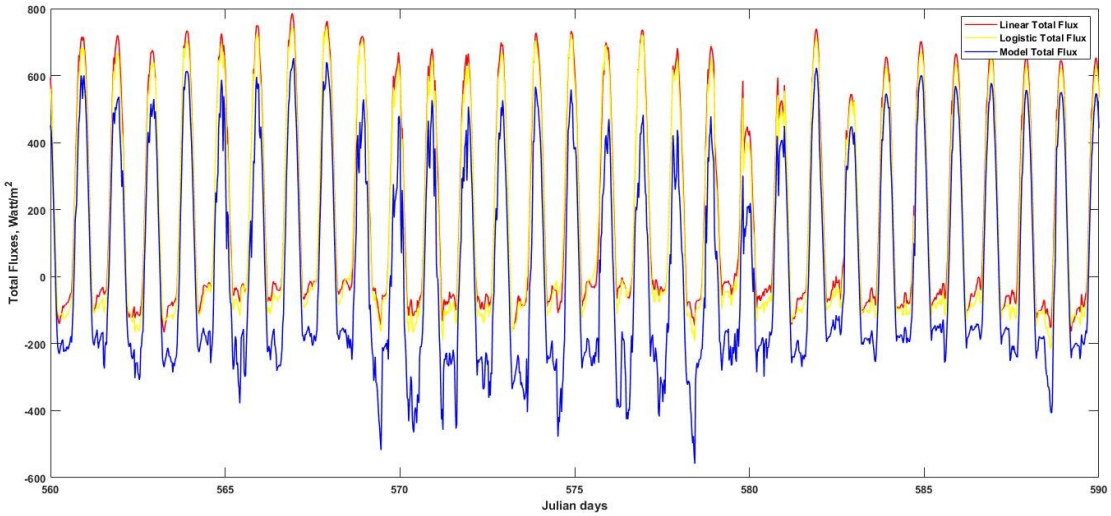

Figure (4-38): Model, logistic and sinusoidal styles for (560-590) Jday.

4.4 Model application: Temperature dynamics in wastewater treatment plants

4.4.1 Study area and dataset

Aeration is the most critical stage in wastewater treatment plant facilities. Aeration removes or modifies constituents to prevent them from interfering with the treatment procedure. Aeration tank looks like a small lake. It is a deep water with a large surface area. The present MATLAB model was developed to solve the advection-dispersion equation. The aeration tank of the wastewater treatment plant in Al-Muamirah in the province of Babylon was the study area. The plant is located in Muamirah, south of the city of Hilla with longitude and latitude of 44.472 and 32.4247, respectively. Figure (4-39) shows Al-Muamirah wastewater treatment plant location on the Google Map. It was established in 1986 with an area of about 70 acres. It receives daily about 107000 m^3/d wastewater. The treatment plant works 24/7 with morning and evening shifts. There are two aeration tanks at the plant. Each tank was divided into five zones to accomplish the adopted finite difference scheme (Makinia et al., 2005). Figure (4-40) reveals the five zones of aeration tanks.

Besides the mentioned inputs (meteorological data, air and water temperature, dew point, wind speed, relative humidity, and cloud cover inputs), other input data were needed to complete the calculation of biological, mechanical, and aeration flux. To calculate aeration flux, data of airflow density, liquid density, the molecular weight of water, latent heat, and vapor pressure of air and water were required. Inputs data of Mass of the substrate removed per day, influent flow rate inputs, and Gibb's free energy for aerobic respiration, nitrification, and de-nitrification were entered to calculate biological flux. Finally, mechanical flux was calculated by the power efficiency.

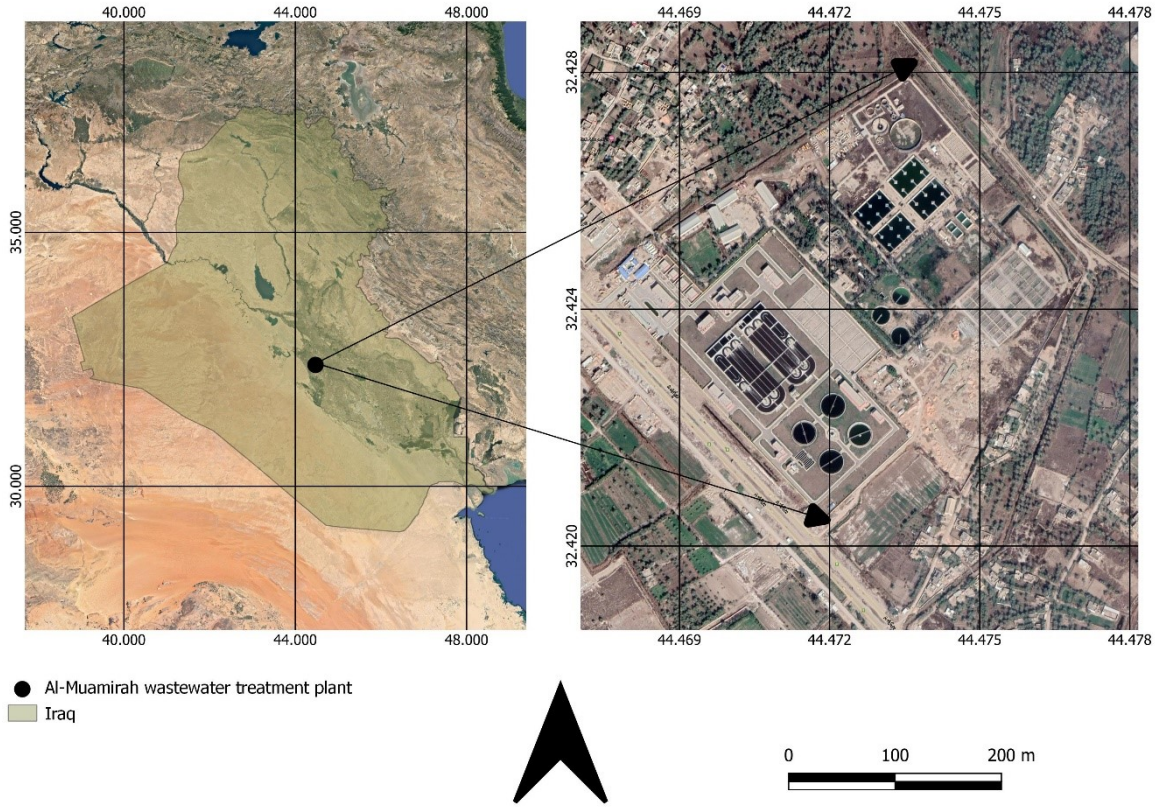

Figure (4-39): Al-Muamirah wastewater treatment plant location retrieved by QGIS.

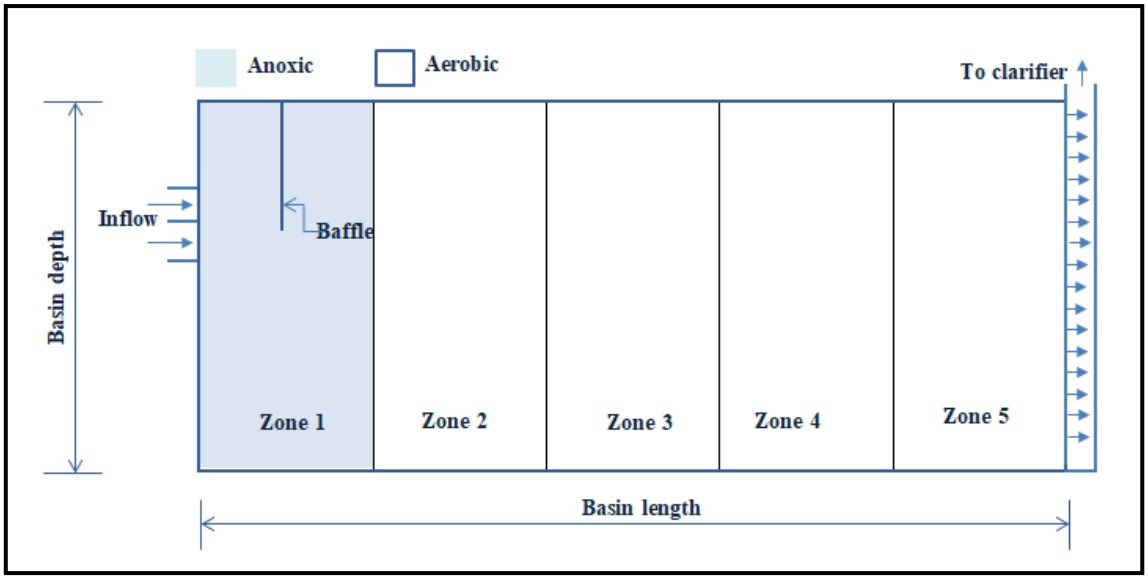

Figure (4-40): Schematic diagram of aeration tank zones.

Consequently, the required input data can be categorized as follows**:**

1. Design data includes included influent, airflow rate, width, length, and depth for the aeration basin, etc.
2. Operation data includes aerator power, airflow rate, etc.
3. Temperature which is isolated separately due to its importance and the wide details.

4.4.2 The numerical scheme

The following numerical scheme was used to solve the advection-dispersion equation adopted for the model (Makinia et al., 2005):

$$V.\frac{T_i^{n+1}-T_i^n}{\Delta t}=U\cdot A\cdot T_{i-1}^n-T_i^n-U\cdot A\cdot T_i^n+EL\cdot A\cdot\frac{T_{i+1}^n-T_i^n}{\Delta x}-EL\cdot A\cdot\frac{T_i^n-T_{i-1}^n}{\Delta x}+\frac{H_t{}_i^n}{\rho_l.C_p}\ldots\ldots\ldots(4-1)$$

T : Temperature of wastewater in the reactor, ^oC.

i: Subscript denoting cell number in the reactor.

n : Superscript denoting time level.

U : Flow velocity in the reactor, m/hr.

A : Cross-sectional area at the inlet to the control volume, m^2.

EL: Longitudinal dispersion coefficient, m^2/hr.

dx: distance along reactor axis, m.

H_t : Net-heat-exchange flux.

ρ_l : Liquid density in the reactor, kg/m^3.

C_p: Water specific heat at constant pressure, J/kg* ^oC.

dt: Time, hr.

V: Reactor volume, m^3.

The net heat exchange flux for the reactor was represented graphically in Fig. (4-41). The net heat flux is the algebraic summation of the radiations below (Wells et al., 2005):

$$H_t = \frac{(H_{sn} + H_{an} + H_{br} - H_e - H_c) * \forall}{h} - H_{aer} + H_{bio} + H_m \ \dots\dots\dots (4-2)$$

Where:

Hsn : Net solar radiation (Watt/m^2) .

Han : Net atmospheric radiation (Watt/m^2).

Hbr : Back long wave radiation (Watt/m^2).

He : Evaporation heat flux (Watt/m^2).

He : Conduction heat flux (Watt/m^2).

h: Reactor depth, m.

$\forall$= Aeration tank volume, m^3.

H_{aer}: Aeration-heat-transfer flux, Watt.

H_{bio}: Biological-processes heat-exchange flux, Watt.

H_m: Mechanical-power-heat-exchange flux, Watt.

The numerical solution of the one-dimensional advection diffusion equation was developed as follows:

$$\frac{\partial T}{\partial t} + u\frac{\partial T}{\partial x} = El\,.\frac{\partial^2 T}{\partial x^2} + \frac{\emptyset}{\rho.Cp.\forall}$$

$$\left[\frac{\partial T}{\partial t} + u\frac{\partial T}{\partial x} = El\,.\frac{\partial^2 T}{\partial x^2} + \frac{\emptyset}{\rho.Cp.\forall}\right].\forall$$

$$\forall\frac{\partial T}{\partial t} + u.\forall.\frac{\partial T}{\partial x} = El.\forall\,.\frac{\partial^2 T}{\partial x^2} + \frac{\emptyset}{\rho.Cp}$$

$$\forall\frac{\partial T}{\partial t} + u.A.(T_i^n - T_{i-1}^n) = El.A\,.\frac{T'_{i+\frac{1}{2}} - T'_{i-\frac{1}{2}}}{\partial x} + \frac{\emptyset}{\rho.Cp}$$

$$\forall\frac{T_i^{n+1} - T_i^n}{\partial t} + u.A.(T_i^n - T_{i-1}^n) = El.A\,.\left(\frac{T_{i+1}^n - T_i^n}{\partial x} - \frac{T_i^n - T_{i-1}^n}{\partial x}\right) + \frac{\emptyset}{\rho.Cp}$$

$$\forall\frac{T_i^{n+1} - T_i^n}{\partial t} + u.A.(T_i^n - T_{i-1}^n) = El.A\,.\left(\frac{T_{i+1}^n - T_i^n}{\partial x} - \frac{T_i^n - T_{i-1}^n}{\partial x}\right) + \frac{\emptyset}{\rho.Cp}\right) * \frac{\partial t}{\forall}$$

$$T_i^{n+1} - T_i^n + u.A\frac{\partial t}{\forall}.(T_i^n - T_{i-1}^n)$$

$$= El.A\frac{\partial t}{\forall}\,.\left(\frac{T_{i+1}^n - T_i^n}{\partial x} - \frac{T_i^n - T_{i-1}^n}{\partial x}\right) + \frac{\emptyset}{\rho.Cp}.\frac{\partial t}{\forall}$$

$$T_i^{n+1} = T_i^n - u.A\frac{\partial t}{\forall}.(T_i^n - T_{i-1}^n) + El.A\frac{\partial t}{\forall}\,.\left(\frac{T_{i+1}^n - T_i^n}{\partial x} - \frac{T_i^n - T_{i-1}^n}{\partial x}\right)$$

$$+\frac{\emptyset}{\rho.Cp}\frac{\partial t}{\forall}$$

$$T_i^{n+1} = T_i^n - u.A\frac{\partial t}{\forall}.(T_i^n - T_{i-1}^n) + El.A\frac{\partial t}{\forall}\,.\left(\frac{T_{i+1}^n - T_i^n - (T_i^n - T_{i-1}^n)}{\partial x}\right)$$

$$+\frac{\emptyset}{\rho.Cp}\frac{\partial t}{\forall}$$

$$T_i^{n+1} = T_i^n - u.A\frac{\partial t}{\forall}.(T_i^n - T_{i-1}^n) + El.A\frac{\partial t}{\forall}.\left(\frac{T_{i+1}^n - T_i^n - T_i^n + T_{i-1}^n}{\partial x}\right) + \frac{\emptyset}{\rho.Cp}\frac{\partial t}{\forall}$$

$$T_i^{n+1} = T_i^n - u.A\frac{\partial t}{\forall}.(T_i^n - T_{i-1}^n) + El.A\frac{\partial t}{\forall}.\left(\frac{T_{i+1}^n - 2T_i^n + T_{i-1}^n}{\partial x}\right) + \frac{\emptyset}{\rho.Cp}\frac{\partial t}{\forall}$$

$$T_i^{n+1} = T_i^n - [u.A.(T_i^n - T_{i-1}^n) + El.A.\left(\frac{T_{i+1}^n - 2T_i^n + T_{i-1}^n}{\partial x}\right) + \frac{\emptyset}{\rho.\ Cp}]\frac{\partial t}{\forall}$$

$$\emptyset = H_t.\frac{\forall}{h} + H_{aer} + H_{bio} + H_m$$

$$\emptyset = \frac{(H_{sn} + H_{an} + H_{br} - H_e - H_c)*V}{h} - H_{aer} + H_{bio} + H_m$$

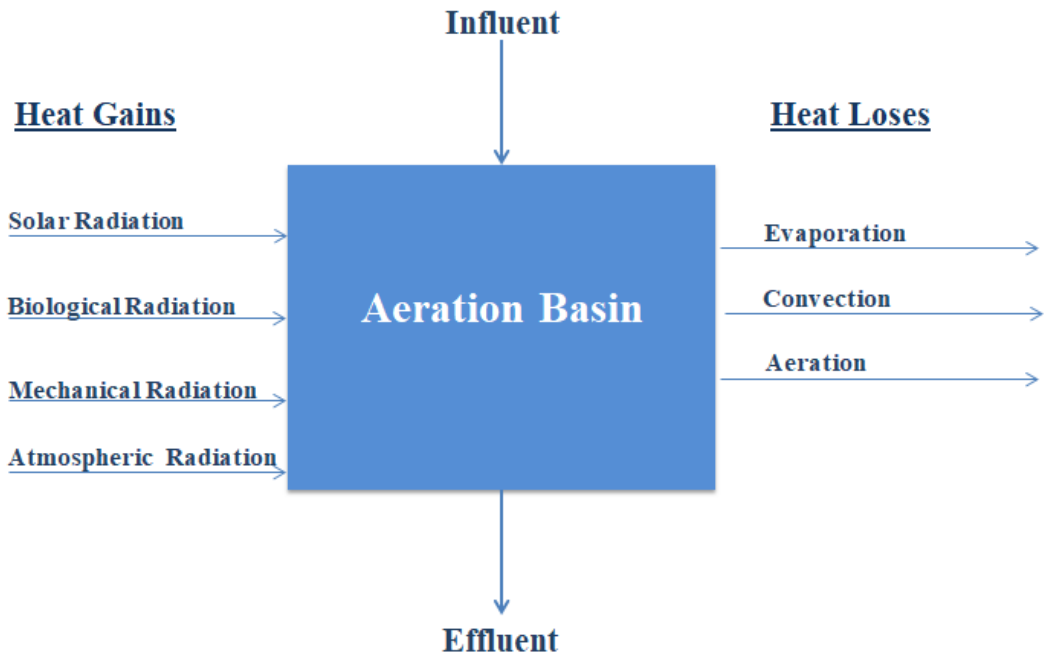

Figure (4-41): Schematic diagram of the heat equilibrium aeration tank.

The three heat fluxes, which are added to the net heat flux, are defined below:

1. *Aeration*, H_{aer}, is the heat loss resulted from the aeration process and composed of two components, sensible loss and latent loss(Talati & Stenstrom, 1990):

$$H_{aer} = H_{as} + H_{al} \quad \ldots\ldots\ldots\ldots\ldots (4-3)$$

$$H_{as} = Q_a \cdot \rho_l \cdot C_p \cdot (T - T_a) \quad \ldots\ldots\ldots\ldots\ldots (4-4)$$

$$H_{al} = \frac{M_w \cdot Q_a \cdot \emptyset_l}{R} \cdot \left\{ \frac{\frac{e_w \cdot [Rh + h_f \cdot (100 - Rh)]}{100} - \frac{e_a \cdot Rh}{100}}{(T_a + 273)} \right\} \ldots\ldots (4-5)$$

Where:

H_{as}: Convective (sensible) heat transfer, Watt.

H_{al}: Evaporative (latent) heat transfer associated with aeration flux, Watt.

Q_a: Airflow rate, m^3/d.

M_w: Molecular weight of water, 18 g/mole.

$\emptyset_l$: Latent heat of evaporation, 2263 J/g.

R: Universal gas constant, 8314.7 J/ (k.mole . K).

e_w: Vapor pressure of water at reactor temperature, Pa.

h_f: Exit-air-humidity factor, h_f = 1.

e_a: Vapor pressure of air at air temperature, Pa.

ρ_l : Liquid density in the reactor, kg/m^3.

C_p: Water specific heat at constant pressure, J/kg* ^oC.

2. *Biological processes*, H_{bio}, is the heat released during exothermic biological processes, such as nitrification, denitrification, and carbon oxidation. It can be figured based on Gibb's free energy terms (Wells et al., 2005):

$$H_{bio} = -\left(\Delta G_1 \cdot \frac{\Delta S}{32} + \Delta G_2 \cdot \frac{8 \cdot S_{ND,in}}{14} + \Delta G_3 \cdot 5 \cdot 0.8 \cdot \frac{S_{ND,in}}{14}\right) \cdot Q \quad \ldots (4-6)$$

Where:

ΔG_1 :Gibb's free energy for aerobic respiration, -110 kJ/e.

ΔS: Mass of the substrate (as chemical-oxygen demand [COD]) removed per day, kg/d.

ΔG_2: Gibb's free energy for nitrification, -43 kJ/e.

$S_{ND,in}$: Soluble-biodegradable-organic-nitrogen concentration in the inlet to the reactor, kg/m^3.

ΔG_3: Gibb's free energy for de-nitrification, -104 kJ/e.

Q: Influent flow rate, m^3/d.

3. *Mechanical energy*, H_m, is the difference between the heat produced during the compression process and the heat added to the reactor, which is represented by the blower inefficiency. It can be computed as (Makinia et al., 2005):

$$H_m = P \cdot (1 - \eta_e) \quad \ldots\ldots\ldots\ldots\ldots (4-7)$$

Where :

P : Power of aerator/compressor, Watt.

η_e: Efficiency of aerator/compressor, 0.4.

4.4.3 Model simulation results

The model was run for 24 hours to estimate the temperatures in the aeration tank based on the available data from Al-Muamirah wastewater treatment plant Table (4-7). Figure (4-42) shows the site measurements and the simulated temperatures. Due to the lack of data in the study location some data

has been enforced. The hypothesis process was within the typical range of that data, and the hypothesis was validated after numerous trials. The model predictions showed good agreement with the real data. The MAE and RMSE values were not high. MAE values was below 0.322 ^{o}C. For the RMSE values, the highest value was 0.771 ^{o}C. The model ability to anticipate aeration basin temperatures is demonstrated by the low errors values. The predicted temperatures for 28/6/2021 were between (29.6 -30.01) ^{o}C. It is also noted that the entry of wastewater represents the entry of the new heat wave that begins to rise gradually until it reaches the exit of the basin, recording its highest value. This process repeats itself each entry.

The estimated wastewater temperature at 10 a.m. on 28/6/2021 for zone 3 was 29.83 ^{o}C, while the actual temperature was 30 ^{o}C. And after two hours later, the estimated temperatures were 29.78 ^{o}C and 29.83 ^{o}C at 11 a.m. and 12 p.m., while the site temperatures were 30.01 ^{o}C and 30.03 ^{o}C, respectively. This means the difference between the site measurement and model estimation was 0.17, 0.23, and 0.2 ^{o}C at 10 a.m., 11 a.m., and 12 p.m., respectively.

Table (4-7): Required data to run model.

Data Name	***Value***			***Data Name***	***Value***
Laboratory Data				***Operational Data***	
ΔS	2.3 (Assumed)			Q	50,000 m^3/d
$S_{ND,in}$	0.005 (Assumed)			U	3 km/hr.
ρ_l	870 kg/ m^3 (Assumed)			P	160 kWatt
Temperatures	***Zone 1***	***Zone 2***	***Zone 3***	Q_a	205 m^3/hr(Assumed)
Temperature at 10 am.	29.8	30	32	C_p	1014 J/kg* ^oC
Temperature at 11 am.	30	30.01	30.02	EL	1100 m^2/hr(Assumed).
Temperature at 12am.	30.01	30.03	30.03	***Model Assumptions***	
Design Data				Δx	30 m
Depth	6.4 m			Δt	1 hr.
Width	62 m			i	5 zones
Length	150 m			n	24 hr.

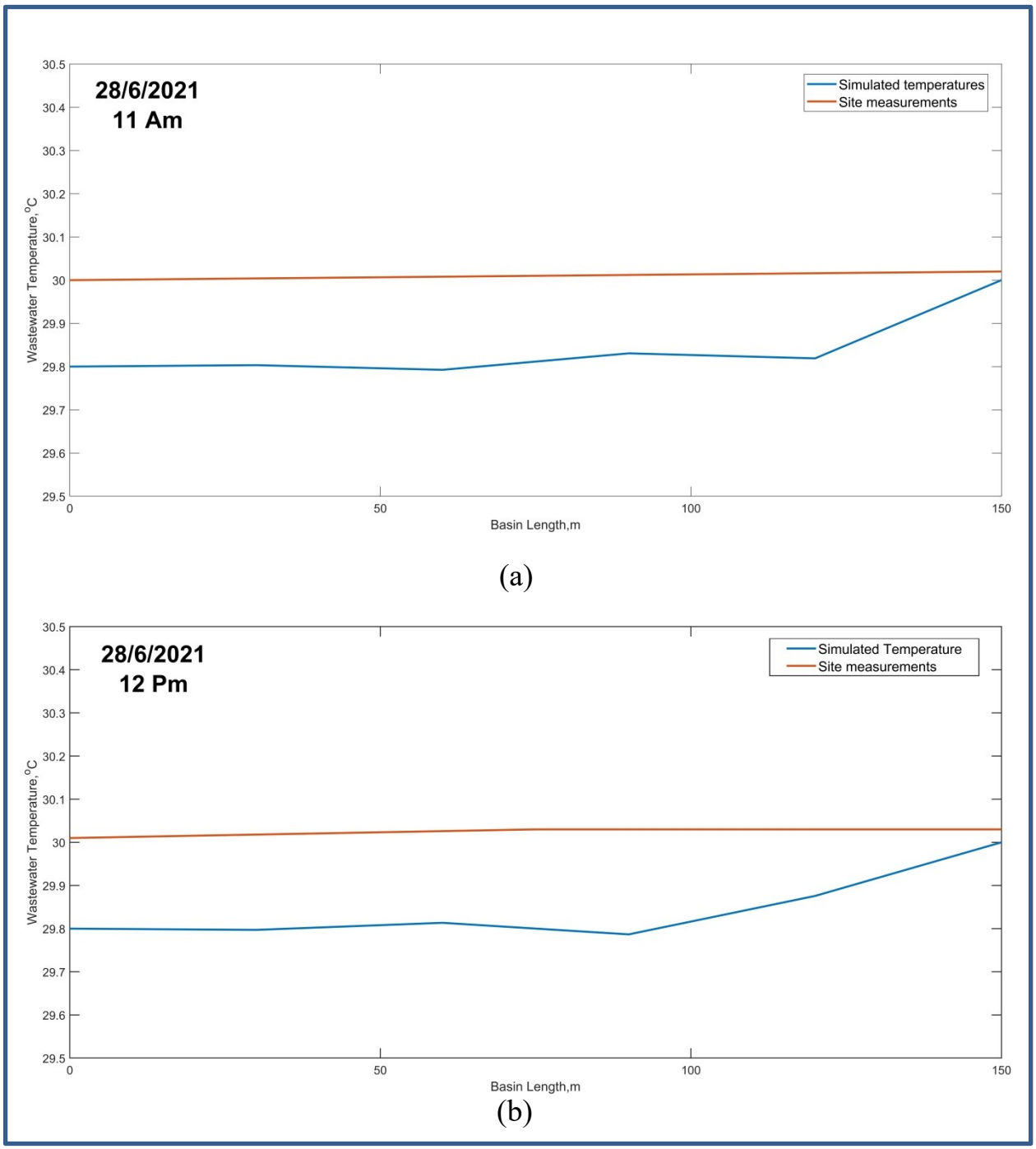

Figure (4-42): The site measurements and the simulated temperatures.

To show the effect of how the model depends on the essential radiations (solar and atmospheric radiation, evaporation, conduction, and back radiations). The radiations (mechanical, biological, and aeration radiations) were separated internally within the code. The outcome of this elimination was displayed in Fig. (4-43) and Table (4-8). The results were, at 10 a.m. was 29.83 ^{o}C, while at

11 a.m. was 29.78 °C. At noon the estimated temperature was 29.83 °C. There is no difference between the temperature computed based on all radiations and the main ones. The MAE and RMSE values were around zero °C for the first four zones, while the MAE and RMSE for the last zone were 0.0017 and 0.0048 °C, respectively. This demonstrates that the results for the present model with its essential radiations are not very different from the results of the original model with its five radiations. MAE and RMSE values are shown in the Table (4-9).

Table (4-8): Wastewater temperatures at zone No.3 (at the middle of the aeration basin) in °C.

Temp. / **Time**	**Actual**	**Estimated with all radiations**	**Estimated with basic radiations**
10 am	30	29.83	29.83
11 am	30.01	29.78	29.78
12 am	30.03	29.83	29.83

Table (4-9): MAE and RMSE values at zones No.1, 3 and 5 in the aeration basin.

Zones		**Zone no.1**	**Zone no3**	**Zone no.5**
Using all radiations	MAE	0.051	0.076	**0.322**
	RMSE	0.102	0.125	**0.770**
Using basic radiations	MAE	0.051	0.080	**0.324**
	RMSE	0.102	0.132	**0.774**

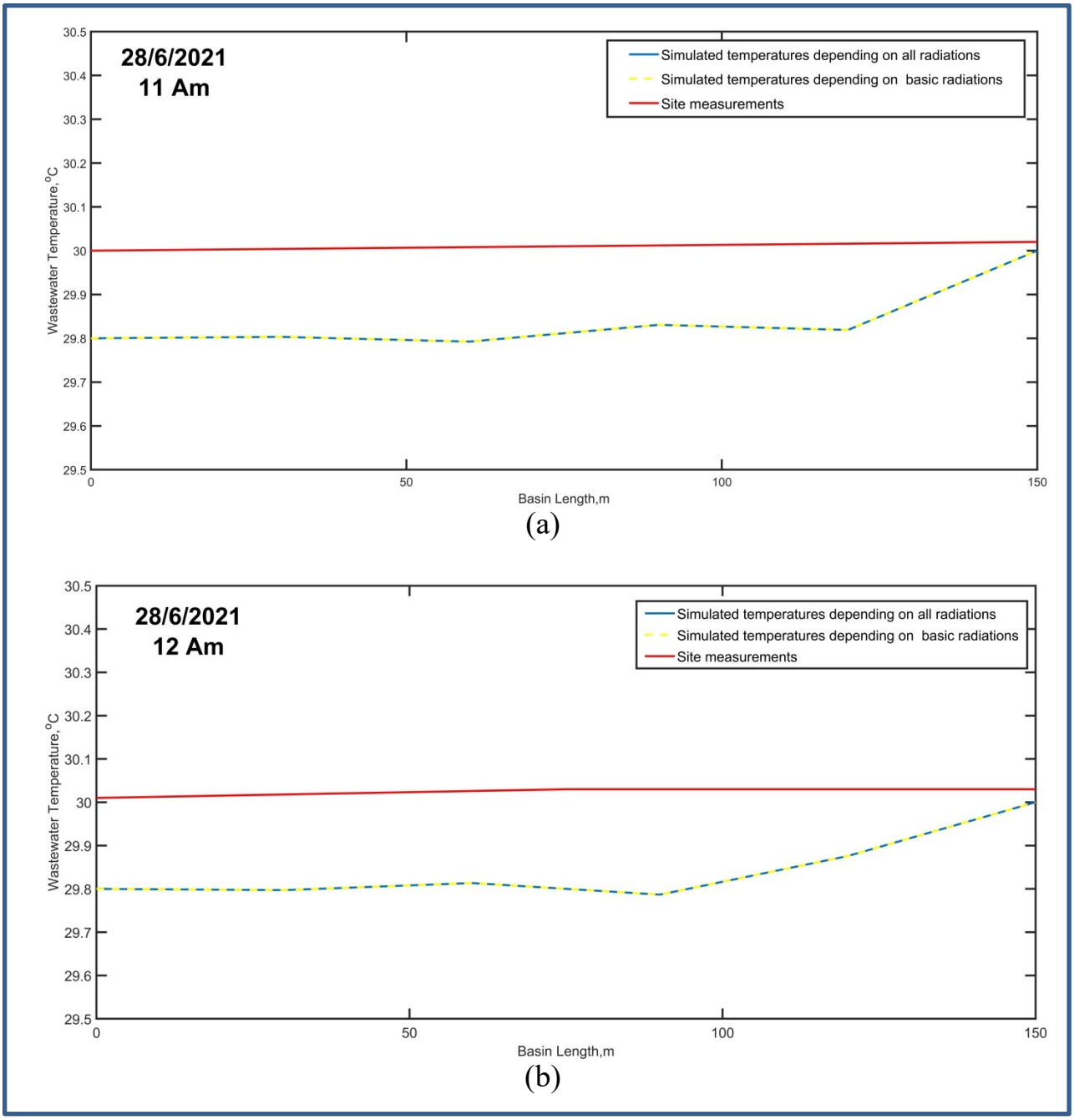

Figure (4-43): The site measurements and the simulated temperatures by all radiations and basic radiations.

CHAPTER FIVE

Conclusions and Recommendations

5.1 Conclusions

A model was built to calculate the atmospheric-water heat fluxes that affect water temperature in surface waterbodies. This study concluded the following results:

1. Model simulation:
    a. Solar radiation flux is more powerful than other fluxes.
    b. Solar radiation flux has the main impact the total heat flux, but its daily fluctuations effect reduces generally. In a big picture, the prominent role of the influence on total heat flow is to the back radiation flux because of its continuous and somewhat stable effect.
    c. Because back radiation flux is a function of water temperature, its curve is identical to the water temperature curve.
    d. Wind speed function is very powerful for calibrating the model. Any change in the wind speed function will cause a change in evaporation and conduction fluxes and that leads to a change in the total heat flux.

2. Air–water regression:
    a. The impacted fluxes are back radiation, evaporation, and conduction. This is due to its dependency on water temperature.
    b. Sinusoidal regression model results are close to logistic regression model even though AME, RMSE, and NSE values denoted that the logistic style is more efficient than the sinusoidal style.

3. Model application: The model implementation of a WWTP aeration tank to calculate water temperature was performed and highlighted the following:
    a. The difference between the site measurements and model

estimations was less than 0.25 ^{o}C.

b. After exclusion fluxes (mechanical, biological and aeration heat fluxes), the model showed very close results with approximately negligible AME and RMSE.

5.2 Recommendations

Future recommendations are:

1. Applying the model to a local waterbody.
2. Linking the model with the advection-diffusion equation for modeling lakes or reservoirs temperature and water quality.
3. Trying different air-water temperatures regression styles.
4. Linking the model with other water quality constituents such as DO, BOD, sediments… etc.
5. Testing the model sensitivity to the atmospheric emissivity.
6. Developing a model to simulate the thermal pollution spreading in the waterbodies.
7. Linking the model with water temperature retrieved by remote sensing technology.
8. Take into account other heat exchange fluxes.

REFERENCES

REFERENCES

REFERENCES

Abdi, R., & Endreny, T. (2019). A River Temperature Model to Assist Managers in Identifying Thermal Pollution Causes and Solhttps://www.mendeley.com/?utm_source=web_importer&utm_campaign=mendeley_logoutions. *Water*, *11*(5), 1060. https://doi.org/10.3390/w11051060

Al-Murib, M., Wells, S., & Talke, S. A. (2017). Estimation of Surface Water Temperature of the Tigris River System in Iraq. *World Environmental and Water Resources Congress 2017*, *May*, 223–233. https://doi.org/10.1061/9780784480632.016

Al-Zubaidi, H. A. M. (2018). *3D hydrodynamic , temperature , and water quality numerical model for surface waterbodies : development , verification , and field case studies* [Portland State University.]. https://doi.org/https://doi.org/10.15760/etd.6384

Al-Zubaidi, H. A. M., & Wells, S. A. (2020). Analytical and field verification of a 3D hydrodynamic and water quality numerical scheme based on the 2D formulation in CE-QUAL-W2. *Journal of Hydraulic Research*, *58*(1), 152–171. https://doi.org/10.1080/00221686.2018.1499051

Annear, R. L., & Wells, S. A. (2007). A comparison of five models for estimating clear-sky solar radiation. *Water Resources Research*, *43*(10). https://doi.org/10.1029/2006WR005055

Augustyn, A., & Rafferty, J. P. (2009). *evaporation | Definition & Facts | Britannica*. https://www.britannica.com/science/evaporation

Benyahya, L., Caissie, D., St-Hilaire, A., Ouarda, T. B. M. ., & Bobée, B. (2007). A Review of Statistical Water Temperature Models. *Canadian Water Resources Journal*, *32*(3), 179–192. https://doi.org/10.4296/cwrj3203179

Berger, C. J., Wells, S. A., & Annear, R. (2005). Laurance lake temperature Model. In *Technical Report EWR-01-04 prepared for Middle Fork Irrigation District.* (Issue 01(04)).

Beschta, R., Bilby, R., Brown, G., Holtby, L., & Hofstra, T. (1987). Stream temperature and aquatic habitat: fisheries and forestry interactions.

REFERENCES

Streamside Management: Forestry and Fishery Interactions, 191–232.

Bowen, I. S. (1926). The Ratio of Heat Losses by Conduction and by Evaporation from any Water Surface. *Physical Review*, *27*(6), 779–787. https://doi.org/10.1103/PhysRev.27.779

Boyd, M., & Kasper, B. (2003). *Analytical Methods for Dynamic Open Channel Heat and Mass Transfer: Methodology for the Heat Source Model Version 7.0*. 204. http://www.deq.state.or.us/wq/TMDLs/tools.htm

Brunt, D. (1932). Notes on radiation in the atmosphere. I. *Quarterly Journal of the Royal Meteorological Society*, *58*(247), 389–420. https://doi.org/10.1002/qj.49705824704

Chen, Y. D., Carsel, R. F., McCutcheon, S. C., & Nutter, W. L. (1998). Stream Temperature Simulation of Forested Riparian Areas: I.Watershed-Scale Model Development. *Journal of Environmental Engineering*, *124*(4), 304–315. https://doi.org/10.1061/(ASCE)0733-9372(1998)124:4(304)

Cole, T. M., & Wells, S. A. (2006). CE-QUAL-W2: A two-dimensional, laterally averaged, hydrodynamic and water quality model, version 3.5. In *Instruction Report EL-95 US Army Engineering and Research Development Center, Vicksburg, MS.* https://pdxscholar.library.pdx.edu/cengin_fac/157/

Deas, M. L., & Lowney, C. L. (2000). *Water Temperature: Modeling Review*. *September*, 113.

Demars, B. O. L., & Manson, J. R. (2013). Temperature dependence of stream aeration coefficients and the effect of water turbulence: A critical review. *Water Research*, *47*(1), 1–15. https://doi.org/10.1016/j.watres.2012.09.054

Demars, B. O. L., Manson, J. R., Ólafsson, J. S., Gíslason, G. M., & Friberg, N. (2011). Stream hydraulics and temperature determine the metabolism of geothermal Icelandic streams. *Knowledge and Management of Aquatic Ecosystems*, *402*(402), 05. https://doi.org/10.1051/kmae/2011046

Edinger, J.E., D. K. B. and J. C. G. (1974). *Heat Exchange and Transport in the Environment*.

Edinger, J. E., & Geyer, J. C. (1974). Heat exchange and taransport in the

REFERENCES

environment. In *Electric power research institute* (Issue 14).

Fink, G., Schmid, M., Wahl, B., Wolf, T., & Wüest, A. (2014). Heat flux modifications related to climate-induced warming of large European lakes. *Water Resources Research*, *50*(3), 2072–2085. https://doi.org/10.1002/2013WR014448

Foreman, M. G. G., James, C. B., Quick, M. C., Hollemans, P., & Wiebe, E. (1997). Flow and temperature models for the Fraser and Thompson Rivers. *Atmosphere-Ocean*, *35*(1), 109–134. https://doi.org/10.1080/07055900.1997.9649587

Grossnickle, S. C., & Canada, N. R. C. (2000). Ecophysiology of northern spruce species: The performance of planted seedlings. In *NRC Research Press* (illustrate). NRC Research Press.

Ji, Z.-G. (2017). *Hydrodynamics and Water Quality*. John Wiley & Sons, Inc. https://doi.org/10.1002/9781119371946

Kalinowska, Monika B., & Rowiński, P. M. (2015). Thermal Pollution in Rivers—Modelling of the Spread of Thermal Plumes. In *GeoPlanet: Earth and Planetary Sciences* (pp. 591–613). https://doi.org/10.1007/978-3-319-17719-9_24

Kalinowska, Monika Barbara. (2019). Effect of water–air heat transfer on the spread of thermal pollution in rivers. *Acta Geophysica*, *67*(2), 597–619. https://doi.org/10.1007/s11600-019-00252-y

Klassen, S., & Bugbee, B. (2015). Shortwave Radiation. In *Energy and Climate in the Urban Built Environment* (Issue 47, pp. 43–57). Routledge. https://doi.org/10.2134/agronmonogr47.c3

Magnus, G. (1844). Versuche über die Spannkräfte des Wasserdampfs. *Annalen Der Physik Und Chemie*, *137*(2), 225–247. https://doi.org/10.1002/andp.18441370202

Makinia, J., Wells, S. A., & Zima, P. (2005). Temperature Modeling in Activated Sludge Systems: A Case Study. *Water Environment Research*, *77*(5), 525–532. https://doi.org/10.2175/106143005x67449

Murray, J. D. (2002). *Mathematical Biology - I. An Introduction | James D. Murray | Springer*. https://www.springer.com/gp/book/9780387952239

Prats, J., Val, R., Dolz, J., & Armengol, J. (2012). Water temperature modeling in the Lower Ebro River (Spain): Heat fluxes, equilibrium

REFERENCES

temperature, and magnitude of alteration caused by reservoirs and thermal effluent. In *Water Resources Research* (Vol. 48, Issue 5). https://doi.org/10.1029/2011WR010379

Rajwa-Kuligiewicz, A., Bialik, R. J., & Rowiński, P. M. (2015). Dissolved oxygen and water temperature dynamics in lowland rivers over various timescales. *Journal of Hydrology and Hydromechanics*, *63*(4), 353–363. https://doi.org/10.1515/johh-2015-0041

Reiser, D. W., & Bjornn, T. C. (1979). Habitat Requirements of Anadromous Salmonids. *U.S. Department of Agriculture*, *October*, 1–54.

Rutherford, J. C., Macaskill, J. B., & Williams, B. L. (1993). Natural water temperature variations in the lower Waikato river, New Zealand. *New Zealand Journal of Marine and Freshwater Research*, *27*(1), 71–85. https://doi.org/10.1080/00288330.1993.9516547

Shanahan, P. (1984). Water temperature modeling: a practical guide. *Environmental Protection Agency*, *U.S. EPA R*(1), 1–25.

Steele, J. G. (1989). High-resolution profiles of temperature and dissolved oxygen in a river. *Hydrobiologia*, *179*(1), 17–24. https://doi.org/10.1007/BF00011926

Steven C. Chapra. (2008). *Surface water-quality modeling*. Waveland Press.

Talati, S. N., & Stenstrom, M. K. (1990). Aeration-Basin Heat Loss. *Journal of Environmental Engineering*, *116*(1), 70–86. https://doi.org/10.1061/(ASCE)0733-9372(1990)116:1(70)

Vannote, R. L., Minshall, G. W., Cummins, K. W., Sedell, J. R., & Cushing, C. E. (1980). The River Continuum Concept. *Canadian Journal of Fisheries and Aquatic Sciences*, *37*(1), 130–137. https://doi.org/10.1139/f80-017

Wang, K., & Dickinson, R. E. (2013). Global atmospheric downward longwave radiation at the surface from ground-based observations, satellite retrievals, and reanalyses. *Reviews of Geophysics*, *51*(2), 150–185. https://doi.org/10.1002/rog.20009

Webb, B. W., & Walling, D. E. (1993). Temporal variability in the impact of river regulation on thermal regime and some biological implications. *Freshwater Biology*, *29*(1), 167–182. https://doi.org/10.1111/j.1365-2427.1993.tb00752.x

REFERENCES

Wells, S. A., Bashkatov, D., & Makinia, J. (2005). Modeling and evaluating temperature dynamics in wastewater treatment plants. *World Water Congress 2005: Impacts of Global Climate Change - Proceedings of the 2005 World Water and Environmental Resources Congress*, *40792*(November 2014), 137. https://doi.org/10.1061/40792(173)137

الخلاصة

مياه الصرف الصحي بالمعيميرة ، تم تشغيل النموذج لمدة 24 ساعة لتقدير درجات الحرارة في خزان التهوية. تم فرض بعض البيانات بسبب نقص البيانات في موقع البحث. كانت البيانات من درجات الحرارة المتوقعة قريبة للغاية من البيانات الحقيقية. كانت قيم AME و RMSE منخفضة نسبيًا. قيم AME و RMSE أقل من 1. وتجدر الإشارة أيضًا إلى أن وصول مياه الصرف الصحي ينذر ببدء موجة حرارة جديدة ، تتكثف باطراد حتى تصل إلى مخرج الحوض ، عندما تصل إلى ذروتها. مع كل إدخال ، تتكرر العملية. توضح قيم الأخطاء المنخفضة قدرة النموذج على التنبؤ بدرجات حرارة حوض التهوية. في الساعة 10 صباحًا يوم 2021/6/28 ، كانت درجة حرارة المياه الثقيلة المقاسة عند منتصف الحوض 30 درجة مئوية ودرجة الحرارة المقدرة بواسطة النموذج 29.79 درجة مئوية. علاوة على ذلك ، قدمت عدة رسومات لدرجات الحرارة المقدرة لحوض التهوية لمدة 24 ساعة.

الخلاصة

التقدير الدقيق لتبادل الطاقة السطحية ومكوناتها هو الأساس لمحاكاة جودة المياه السطحية ، خاصة في البحيرات والخزانات ، لأن انتقال الحرارة بين الماء والهواء يؤثر بشكل مباشر على الطبقات الحرارية. في هذا البحث ، استنادًا إلى سطح الماء وبيانات الأرصاد الجوية من بحيرة لورانس ، تُستخدم طريقة مصطلح تلو الاخر لنمذجة تدفق الحرارة (الإشعاع الشمسي والجوي والإشعاع العكسي والتبخر والتوصيل). استخدم بيئة MATLAB لتطوير الكود ومحاكاة النتائج. تعد القدرة على إبراز مساهمة كل مكون من مكونات التدفق السمة الرئيسية للنموذج ، حيث تقدم دليلاً على التداخل القوي بين سطح الماء والغلاف الجوي.

في فترة الدراسة (487-670) يوماً شمسياً. وأظهرت النتائج أن الطاقة الشمسية الصيفية هي الأعلى كثافة وبلغت ذروتها 842.05 (واط / م ^{2}) في اليوم الشمسي 540.91 . وبسبب الظاهرة الطبيعية لشروق وغروب الشمس ، فإن الطاقة الشمسية لها تقلبات يومية. انه يتراوح بين 0 (وات / م^2) ليلاً ويصل إلى ذروته اليومية عند الظهيرة تقريبًا. على الرغم من أن القيمة القصوى للدفق الحراري البخاري سجلت عند اليوم الشمسي 578.44 هي(359.77 واط / م ^{2})، فإن أدنى قيمة للتدفق الحراري عبر التوصيل عند اليوم الشمسي 655.54 هي (126.039 واط / م ^{2}). يتقلب تدفق الإشعاع الراجع أقل من التدفقات الأخرى. يعود هذا إلى اعتماده على عامل واحد متغير ، وهو درجة حرارة الماء. القيمة القصوى المسجلة للإشعاع الخلفي (410.06 وات / م ^{2}) مرتبطة بدرجة حرارة الماء القصوى (21.5 درجة مئوية). محاكاة النموذج تُظهر تأثير منحنى الجرسي للإشعاع الشمسي على منحنى التدفق الحراري الكلي في وقت قصير.

يطبق النموذج اقتراح Edinger لمعاملات سرعة الرياح (b1 = 9.4، b2 = 0 و b3 = 0.46). تم إجراء معايرة لكل معامل. وجد أن منحنيات المعايرة الناتجة تحاكي منحنى النموذج ولكن في نطاقات مختلفة. لمزيد من المرونة ، تم تطبيق اقتراحات أخرى من الباحثين على النموذج. تم اكتشاف أن (Ahsan & Blumberg، 1999؛ Arifin et al.، 2016؛ Ji، 2017) كان النموذج المقترح أقرب إلى الوضع من الاقتراحات الأخرى. أيضًا ، تم أخذ معامل حماية الرياح (WSC)على أنه مضاعف سرعة الرياح.

من أجل ربط النموذج المطور بمعادلة التأفق والتشتت ، تم إجراء دراسة حالة بناءً على بيانات ميدانية من حوض تهوية في محطة معالجة مياه الصرف الصحي بالمعيميرة. استنادًا إلى

جمهورية العراق
وزارة التعليم العالي والبحث العلمي
جامعة بابل
كلية الهندسة
قسم هندسة البيئة

نمذجة التبادل الحراري بين الهواء والماء في المسطحات المائية: خوارزميات وتطبيقات

رسالة مقدمة الى قسم هندسة البيئة/ كلية الهندسة في جامعة بابل كجزء من

متطلبات نيل درجة الماجستير في الهندسة/ هندسة البيئة

إعـــداد

داليـــا سعـــد عبـــد زيـــدجدوع

بإشـــراف

أ.م.د. حســـين علي مهدي الزبيـــدي